DENTAL MATERIALS 35 (2019) 310–327

Available online at www.sciencedirect.com

ScienceDirect

journal homepage: www.intl.elsevierhealth.com/journals/dema

Dental pulp stem cells in chitosan/gelatin scaffolds for enhanced orofacial bone regeneration

Athina Bakopoulou[a], *Anthie Georgopoulou*[b], *Ioannis Grivas*[c], *Chryssa Bekiari*[c], *Oleg Prymak*[d], *Kateryna Loza*[d], *Matthias Epple*[d], *George C. Papadopoulos*[c], *Petros Koidis*[a], *Maria Chatzinikolaidou*[b,e,*]

[a] *Department of Prosthodontics, School of Dentistry, Faculty of Health Sciences, Aristotle University of Thessaloniki (A.U.Th), Greece*

[b] *Department of Materials Science and Technology, University of Crete, Heraklion, Greece*

[c] *Department of Anatomy, Histology & Embryology, School of Veterinary Medicine, Faculty of Health Sciences, A.U.Th, Greece*

[d] *Inorganic Chemistry & Center for Nanointegration Duisburg-Essen (CeNIDE), University of Duisburg-Essen, Germany*

[e] *Institute of Electronic Structure and Laser (IESL), Foundation for Research and Technology Hellas (FORTH), Heraklion, Greece*

ARTICLE INFO

Article history:
Received 8 June 2018
Received in revised form
19 September 2018
Accepted 20 November 2018

Keywords:
Dental pulp stem cells
Bioinspired chitosan/gelatin scaffolds
Orofacial bone regeneration

ABSTRACT

Objective. Biomimetic chitosan/gelatin (CS/Gel) scaffolds have attracted great interest in tissue engineering of several tissues. However, limited information exists regarding the potential of combining CS/Gel scaffolds with oral cells, such as dental pulp stem cells (DPSCs), to produce customized constructs targeting alveolar/orofacial bone reconstruction, which has been the aim of the present study.

Methods. Two scaffold types, designated as CS/Gel-0.1 and CS/Gel-1, were fabricated using 0.1 and 1% (v/v) respectively of the crosslinker glutaraldehyde (GTA). Scaffolds (n = 240) were seeded with DPSCs with/without pre-exposure to recombinant human BMP-2. *In vitro* assessment included DPSCs characterization (flow cytometry), evaluation of viability/proliferation (live/dead staining, metabolic-based tests), osteo/odontogenic gene expression analysis (qRT-PCR) and structural/chemical characterization (scanning electron microscopy, SEM; energy dispersive X-ray spectroscopy, EDX; X-ray powder diffraction, XRD; thermogravimetry, TG). *In vivo* assessment included implantation of DPSC-seeded scaffolds in immunocompromised mice, followed by histology and SEM-EDX. Statistical analysis employed one/two-way ANOVA and Tukey's *post-hoc* tests (significance for $p < 0.05$).

Results. Both scaffolds supported cell viability/proliferation over 14 days in culture, showing extensive formation of a hydroxyapatite-rich nanocrystalline calcium phosphate phase. Differential expression patterns indicated GTA concentration to significantly affect the expression of osteo/odontogenic genes, with CS/Gel-0.1 scaffolds being more effective in upregulating *DSPP*, *IBSP* and *Osterix*. *In vivo* analysis demonstrated time-dependent

* *Corresponding author at*: Department of Materials Science and Technology, University of Crete, Heraklion, Greece.
E-mail address: mchatzin@materials.uoc.gr (M. Chatzinikolaidou).

https://doi.org/10.1016/j.dental.2018.11.025

production of a nanocrystalline, mineralized matrix at 6, 8 and 10 weeks, being more prominent in constructs bearing rhBMP-2 pre-treated cells. The latter showed higher amounts of osteoid and fully mineralized bone, as well as empty space reduction.

Significance. These results reveal a promising strategy for orofacial bone tissue engineering.

1. Introduction

The regeneration of alveolar bone defects to restore aesthetics and function in a predictable manner while offering a sustainable treatment outcome remains a major challenge still to be addressed despite recent advances in regenerative treatments. Alveolar bone defects may vary in nature; being associated with chronic inflammatory diseases, such as periodontitis or peri-implantitis, injuries, congenital disorders or resorption of the alveolar bone following tooth loss, all leading to noticeable deformity, impaired function and an overall compromised quality of life for patients; this latter being further aggravated by an increasingly ageing population [1].

Currently, treatment modalities are based on applying different types of bone grafts such as autografts, allografts, xenografts and alloplasts, in combination with barrier membranes and various growth factors. These still bear certain limitations in fulfilling the morphological and functional demands of three-dimensional structures, such as the complicated architecture of the periodontal apparatus, or the challenging nature of peri-implant and alveolar bone defects [2]. Moreover, they have often proved somewhat unsatisfactory regarding cost, time of treatment and delivered outcomes [3], thus underlining the need for developing alternative therapies incorporating tissue engineering (TE)-based strategies for clinical application [4].

A number of studies have explored the feasibility of these novel clinical therapeutic procedures for reconstructing intra-oral osseous defects and promoting bone formation [5]. Previous studies by other groups [6], as well as ours [7], have developed clinical-grade preparations of oral mesenchymal stem cells (MSCs), including dental pulp stem cells (DPSCs) and alveolar bone marrow MSCs (aBMMSCs), under good manufacturing practice-compliant (cGMP) conditions, to meet the regulatory requirements for transplantation into humans. Further studies have used TE-based strategies by combining various components of the TE triad (*i.e.* scaffolds, stem cells and growth factors) to restore periodontal, peri-implant and alveolar bone defects [8] but with variable treatment outcomes. However, a major challenge still remaining is to develop scaffold materials that would not only support stem/progenitor cell survival and differentiation stimulating bone formation, but also be easily handled and shaped to accommodate small but quite complex defects encountered in periodontal intrabony or peri-implant lesions, while preserving soft tissue architecture and healing without triggering adverse local reactions or impairing endogenous healing by the host. In this respect, there is still an open call for an exemplary scaffold material fulfilling these requirements.

Natural blends combining chitosan and gelatin have previously been investigated as promising scaffold materials for mineralized tissue – primarily bone – regeneration [4]. Chitosan, a natural copolymer of glucosamine and N-acetylglucosamine [4], is today a component in TE applications, gene therapy and other biomedical areas by virtue of its unique properties, including biocompatibility, stability, sterilizability, biodegradability, antimicrobial and immunostimulatory properties [9,10]. Through its resemblance to the glycosaminoglycans (GAGs) belonging to the natural extracellular matrix (ECM) materials, chitosan also provides a biomimetic microenvironment fostering cell growth, while its osteoconductive properties are capable of supporting stem/progenitor cell osteogenic differentiation and biomineralization [11,12].

Blending chitosan with other biomaterials like gelatin is effective in improving its deficiencies regarding mechanical strength and initial cell attachment [13]. Gelatin is a protein fragment obtained by the partial degradation of collagen fibres. Its many advantages, including biocompatibility, low antigenicity, biodegradability, hydrogel properties and low-cost availability, have led to its wide availability in TE [13]. The presence of the integrin recognition motif Arg–Gly–Asp (RGD) in gelatin also favours the initial cell adhesion [14]. Chitosan/gelatin (CS/Gel) blends offer the possibility of combining these properties and have been proposed as scaffolding materials for regenerating bone [15,16], as well as other tissues, such as cartilage [17], skin [18], and peripheral nerves [19]. However, to date, only limited information exists regarding the potential of combining these blends with oral MSCs to produce customized constructs for application to different types of alveolar bone defects.

DPSCs represent a very promising oral MSC source, potentially with great importance for Regenerative Dentistry [20]. These cells have been evaluated for their *in vitro* multilineage differentiation potential for osteo/odontogenic, adipogenic, chondrogenic, neurogenic, angiogenic and myogenic lineages [21], while *in vivo* studies have confirmed their enhanced potential to reconstitute mineralized tissues, including bone [22] and dentine/pulp complex [23]. Moreover, DPSCs have been considered ideal candidates for TE-based strategies in the craniofacial region because they share the same neural crest derived embryological origin and consequent similar gene expression patterns [21].

Based on the above, this study aimed to evaluate the potential of crosslinked CS/Gel scaffolds produced by freeze-drying to act as a porous microenvironment promoting attachment, viability and osteo/odontogenic differentiation of DPSCs, leading to abundant production of mineralized tissue with chemical and structural characteristics mim-

icking those of natural bone. It has been hypothesized that tuning the crosslinking density of the CS/Gel scaffolds would affect the biological responses of DPSCs. The second hypothesis was that exogenous induction by means of the major osteogenesis related growth factor BMP-2, would foster the osteo/odontogenic differentiation and biomineralization potential, both *in vitro* and *in vivo*.

2. Materials and methods

2.1. Synthesis of chitosan/gelatin (CS/Gel) scaffolds

CS/Gel scaffolds were prepared according to a modified protocol based on Chiono et al. [9], by dissolving 2% (w/v) chitosan in a 1% (v/v) acetic acid solution and 2% (w/v) gelatin in ultrapure demineralized water at 50 °C. The two solutions were mixed in the ratio of 2:3 chitosan/gelatin respectively, and stirred for 2 h at 50 °C [12]. Glutaraldehyde (GTA) was added to the solution as a crosslinking agent for the two components at different concentrations ranging from 0.1 to 2% (w/v). The mixture was kept under agitation at 50 °C until gelation. Subsequently, 400 μl of this mixture were placed per well in a 24-well plate to produce 40:60% CS:Gel scaffolds. These were then frozen at −20 °C and lyophilized for 24 h. The lyophilized scaffolds were neutralized by using 0.1 N NaOH, rinsed thoroughly with ultrapure water until the pH was neutral and, finally, with phosphate buffer saline (PBS) overnight prior to placing in a vented oven for 24 h at 37 °C.

2.2. Characterization of the CS/Gel scaffolds

2.2.1. Scanning electron microscopy (SEM)

The morphology of scaffolds was observed from sample surfaces and cross sections by SEM. Both scaffold types were fixed with 2% (v/v) para-formaldehyde for 30 min and dehydrated in increasing concentrations (30–100% v/v) of ethanol in water. The samples were dried in a critical point drier (Baltec CPD 030), sputter-coated with a 20 nm thick layer of gold-palladium (Baltec SCD 050) and observed under a SEM (JEOL JSM-6390 LV) at an accelerating voltage of 15–20 kV. The average pore size of the scaffolds was evaluated from direct geometrical measurements on the SEM images.

2.2.2. Fourier transform infrared spectroscopic analysis (FTIR)

FTIR analysis of the CS/Gel scaffolds was performed using an optical spectrometer (Nicolet 6700, Thermo Electron Corporation) within the wave number region 500–4000 cm^{-1}. The spectral data were collected and numerical values were transferred to Origin software for graphic presentation.

2.2.3. Degradation, porosity and swelling analysis

In vitro degradation of the CS/Gel crosslinked scaffolds was assessed by immersing them in 10 ml PBS at pH 7.4 and incubating at 37 °C. The scaffolds were removed from the medium at day (d) 3 and subsequently every seven days and then freeze-dried overnight before weighing with a precision balance using the following formula:

$D = (W_0 - W_1)/W_0$, where W_0 is the initial weight of dried scaffolds and W_1 is the weight of scaffolds at different time points following immersion and freeze-drying. The values were expressed as means ± standard error (SE; n = 5).

The porosity of the CS/Gel-0.1 and CS/Gel-1 scaffolds was measured by a liquid displacement method [24]. The volume V_0 and weight W_0 of the dry scaffold were measured and then it was immersed in ethanol until saturation by absorbing ethanol. The scaffold was weighted again and its weight was recorded as W_1. The porosity of the scaffold was calculated according to the formula: % porosity = $(W_1 - W_0)/(\rho V_0) \times 100$, where ρ is the density of ethanol. The values were expressed as means ± standard error (n = 5).

The ability of lyophilized crosslinked CS/Gel scaffolds to absorb water was determined by immersing them for 30 min in deionized water at room temperature. The excess water was removed and their weight was recorded in equilibrium. The percentage water uptake was calculated using the following formula: $W = W_w - W_0/W_0$, where W_0 is the initial weight of the dried scaffolds and W_w is the equilibrium weight of wet scaffolds in water. The values were expressed as means ± standard error (n = 4).

2.3. Establishment of DPSC cultures

DPSC cultures were developed from wisdom teeth of three young healthy donors (1. 17 years old, female donor; 2. 19-years-old, female donor; and 3. 19 years-old, male donor) using the enzymatic dissociation method, as previously described [25]. One wisdom tooth per donor was used for the establishment of each culture. The study was approved by the Institutional Ethics Committee (number 322/15-4-2013), while all patients signed an informed consent. Briefly, impacted third molars were thoroughly washed after extraction and drilled through the cementum-enamel junction to reveal the pulp chamber. Then, the pulp tissue was retrieved, thoroughly minced and digested by means of a collagenase I (3 mg/ml) and dispase II (4 mg/ml) buffer (Invitrogen, Karlsruhe, Germany) for 45 min at 37 °C. The cells were cultured with a-MEM (Minimum Essential Media) medium (Invitrogen), supplemented with 15% fetal bovine serum (FBS, Invitrogen), 100 mM L-ascorbic acid phosphate (Sigma–Aldrich, Steinheim, Germany) and antibiotics/antimycotics (Complete Culture Medium, CCM) before incubating at 37 °C in 5% CO_2. DPSCs in passage 2–6 from three donors were used for the *in vitro* experiments, while DPSCs from two of these donors were further used for the *in vivo* experiments.

2.4. Immunophenotypic profiles of DPSC cultures

DPSCs were analyzed by flow cytometry for mesenchymal (STRO-1, CD146, CD90/Thy-1, CD73, CD49f/a6-integrin), neural (Nestin), endothelial (CD105/endoglin, CD106/VCAM), embryonic (SSEA-1, 3, -4, Nanog, Oct3/4) and hematopoietic (CD34, CD45, CD117/c-Kit) stem cell (SC) markers, as previously described [25]. Single cell suspensions obtained by culture trypsinization were labelled or surface markers with fluorochrome-conjugated antibodies: STRO-1-FITC (fluorescein isothiocyanate), CD146-PE (phycoerythrin), CD90-FITC,

CD73-PE, CD49f-APC (allophycocyanin), CD105-FITC, CD106-APC, SSEA-1-PE, SSEA-3-PE, SSEA-4-FITC, CD34-APC, CD45-PE, c-kit/CD117-PerCP-Cy5.5 (Peridinin–*Chlorophyll*–Protein Complex), (all from BioLegend, Fell, Germany). For detection of intracellular markers (Nestin, Nanog and Oct3/4), the cells were fixed with a 4% paraformaldehyde, permeabilized with 0.1% saponin buffer (BD Biosciences) and then labelled with nestin-APC (RnD Systems, Minneapolis, USA), Nanog-PE and Oct3/4-Alexa Fluor 647 antibodies (Biolegend). After staining and washing of the cells with a FACS buffer (PBS + 1% BSA + 0.1% NaN_3), they were analyzed by means of a Guava® easyCyte 8HT Benchtop Flow Cytometer (Merck Millipore, Billerica, Massachusetts, U.S.A.). A total of 50,000 events/sample were acquired. Data were analyzed using Summit 5.1 software (version 5.1 for Windows, Beckman Coulter, Inc., Krefeld, Germany).

2.5. Seeding of DPSCs into the CS/Gel scaffolds and evaluation of cell attachment, morphology and viability/proliferation

For the *in vitro* experiments, CS/Gel scaffolds cross-linked with two different GTA concentrations, *i.e.* 0.1% (v/v) (designated as CS/Gel-0.1) and 1% (v/v) (designated as CS/Gel-1), were seeded with DPSCs at 10^6 cells/scaffold. Before cell seeding, the scaffolds were incubated for 24 h with CCM at 37 °C and 5% CO_2, to allow their initial wetting with the serum containing medium, as well as pH equilibration at values between 7.2 and 7.4. Each scaffold was then loaded with 100 μl CCM containing 10^6 DPSCs and initially incubated for 1 h at 37 °C and 5% CO_2 before been fully covered with 1 ml CCM/well.

After 24 h, the morphological characteristics of DPSCs inside the CS/Gel scaffolds (CS/Gel-0.1 and CS/Gel-1) were examined by SEM. Cell viability/proliferation was evaluated by means of a metabolic-based test (MTT assay) at 1, 2, 3, 7 and 14 days post-seeding. In addition, live/dead fluorescent staining (Calcein AM/Ethidium Homodimer-EthD1 staining) was performed at 3, 7 and 14 days after cell seeding to evaluate the ratio of live/dead cells inside the constructs by means of confocal microscopy.

In more detail:

2.5.1. Evaluation of initial cell attachment and morphological characteristics by SEM

For SEM observation, the DPSC/scaffold constructs were washed with PBS and processed as described in Section 2.2.1.

2.5.2. Assessment of cell viability/proliferation based on metabolic activity

For this purpose, the MTT [3-(4,5-dimethylthiazol-2-yl)-2,5-diphenyltetrazolium bromide] assay was used, as previously described [25]. The DSPC/scaffold constructs were initially loaded with 2.5×10^5 cells/scaffold. After 1, 2, 3, 7 and 14 days, MTT (0.5 mg/ml in CCM) was added to each cell/scaffold construct and incubated for 4 h at 37 °C and 5% CO_2. The MTT insoluble formazan was then dissolved by means of DMSO that was applied for 2–4 h to the constructs at 37 °C. The optical density (OD) was measured against blank (DMSO) at a wavelength of 545 nm and a reference filter of 630 nm by an ELISA reader (Epock, Biotek, Biotek instruments, Inc., Vermont, U.S.A). Cell-free scaffolds incubated under the same conditions were used as reference controls and their OD values were subtracted from those obtained from the corresponding DPSC/scaffold constructs.

2.5.3. Evaluation of the live to dead cell ratio by confocal microscopy

The DPSC/scaffold constructs were labelled with Calcein AM/EthD1 fluorescent dyes. Stained constructs were observed under a confocal microscope (Leica Microsystems, Wetzlar, Germany). Approximately 25–30 serial sections were obtained and the z-stacked images produced. Quantification of the % percentage of living and dead cells was performed by means of the Image J colour pixel counter plug in.

2.6. Evaluation of the in vitro osteo/odontogenic differentiation potential of DPSC-seeded CS/Gel scaffolds by real-time reverse-transcription polymerase chain reaction analysis (qPCR)

For qPCR experiments, DPSCs were loaded into the CS/Gel scaffolds (CS/Gel-0.1 and CS/Gel-1), as described in Section 2.5, and allowed to attach for 24 h. Two experimental groups/scaffold type were analysed: in the first group, the DPSC/scaffold constructs were exposed to CCM for 14 day with medium been changed every other day; while in the second group, the cells were pre-induced by single application of 100 ng/ml recombinant human (rh)-BMP-2 (Invitrogen) for 24 h and then further cultured with CCM until the end of the experiments (14 day). The rationale of the second setting was to verify whether a single external application of the osteoinductive agent BMP-2, as previously described [26] would promote the osteo/odontogenic shift and biomineralization phenomena exerted by DPSCs inside the constructs.

RNA isolation was performed after 7 and 14 days in culture to be used for cDNA synthesis and qPCR analysis of the expression of several osteo/odontogenesis-related genes. The Nucleospin™ RNA isolation kit (Macherey Nagel, Düren, Germany) and a Superscript first-strand synthesis kit (Invitrogen) were used for RNA isolation and cDNA conversion respectively according to manufacturer's instructions. The SYBR-Select PCR Master Mix (Applied Biosystems, Foster City, CA)was used for qPCR reactions that were performed in a Step One Plus thermal cycler (Applied Biosystems) beginning with two incubation steps at 50 °C for 2 min and at 95 °C for 2 min and followed by 40 cycles of PCR, each including denaturation for 15 s at 95 °C and combined annealing/extension for 1 min at 60 °C. The Primer-Blast software (http://www.ncbi.nlm.nih.gov/BLAST) was used for the primer design, as shown in Table 1. The results were adjusted by amplification efficiency (LinRegPCR) and were normalized to the two most stable housekeeping genes evaluated by geNorm (succinate dehydrogenase complex, subunit A, flavoprotein-SDH-A and beta-2-microglobulin-B2M).

2.7. Mineralized tissue characterization inside the DPSC-seeded CS/Gel scaffolds

In this set of *in vitro* biomineralization experiments, the same experimental setting (2 groups/scaffold type) was

Table 1 – Primers designed for the real-time PCR analysis of several osteo/odontogenic differentiation-related genes and the respective amplicon sizes of the PCR products.

Gene symbol	Forward (5′–3′)	Reverse (5′–3′)	Amplicon size (bp)
DSPP	GCTGGCCTGGATAATTCCGA	CTCCTGGCCCTTGCTGTTAT	135
BMP-2	GGAACGGACATTCGGTCCTT	AGTCCGTCTAAGAAGCACGC	100
IBSP	AAGGACAAGGCTACGATGGC	CGGATGCAAAGCCAGAATGG	97
BGLAP	GACTGTGACGAGTTGGCTGA	AAGAGGAAAGAAGGGTGCCT	137
OSTERIX (SP7)	ATCCAGCCCCCTTTACAAGC	TAGCATAGCCTGAGGTGGGT	78
ALP	CCGTGGCAACTCTATCTTTGG	CAGGCCCATTGCCATACAG	89
B2M	TGTCTTTCAGCAAGGACTGGT	ACATGTCTCGATCCCACTTAAC	138
SDHA	GCATGCCAGGGAAGACTACA	GCCAACGTCCACATAGGACA	127

used, as described for the qPCR experiments (Section 2.6). DPSC/scaffold constructs were cultured with CCM, additionally supplemented with 5 mM β-glycerophosphate (β-GP) as an external phosphate source. Medium change was performed every 2 day for a total of 8 weeks (w). Cell-free scaffolds exposed to the same medium were used as controls for this assay to exclude spontaneous calcium phosphate (CaP) precipitation due to the addition of phosphates to the culture medium. After 4 and 8 weeks, samples of the different experimental groups were subjected to SEM examination combined with energy dispersive X-ray spectroscopy (SEM-EDX), X-ray diffraction analysis (XRD), Rietveld refinement and thermogravimetry (TG). Specifically:

2.7.1. *SEM–EDX analysis*

SEM–EDX was used to perform structural characterization of DPSC-seeded scaffolds and surface elemental composition analysis, respectively. The DPSC/scaffold constructs of each experimental group/time-point were washed with PBS and processed as described in Section 2.2.1. SEM examination was performed with an ESEM Quanta 400 FEG instrument (FEI), equipped with EDX spectroscopy (EDX; Genesis 4000, SUTW-Si(Li) detector) operating in a high vacuum with gold/palladium-sputtered samples.

2.7.2. *XRD and Rietveld refinement analysis*

XRD was used to assess and further characterize the mineralized tissue produced inside the DPSC-seeded scaffolds. The constructs, first rolled into flat samples, were deposited on a silicon single crystal sample holder to minimize scattering and finally fixed by paraffin wax. All samples were rotated in Bruker D8 Advance instrument (Bragg–Brentano geometry with CuKα radiation, 1.54 Å, 40 kV and 40 mA) and investigated from 5 to 90° 2θ with a step size of 0.01° and a counting time of 0.6 s at each step. For the qualitative phase analysis, a software Diffrac. Suite EVA V1.2 from Bruker was used, and the patterns of hydroxyapatite, HAP (#09-0432) and paraffin (#40-1995) from the ICDD database were used as references. For the quantitative analysis and determination of lattice parameters *a*, *c* (hexagonal structure of HAP) and crystallite size *D* of formed CaP, Rietveld refinement by means of the program package TOPAS 4.2 from Bruker was applied. It should be noted that for each Rietveld refinement, the instrumental correction, as determined with a standard powder sample LaB6 from NIST (National Institute of Standards and Technology) used as standard reference material (SRM 660b; a(LaB6) = 4.15689 Å), was taken into account.

2.7.3. *Determination of inorganic content inside the DPSC/scaffold constructs*

The DPSC/scaffold constructs were exposed to a high temperature (1000 °C, oxygen atmosphere) and the organic fraction was oxidized (volatilized), leaving only the inert fraction (unoxidized). The experiments were carried out with a Netzsch STA 449 F3 Jupiter instrument in a dynamic oxygen atmosphere at a heating rate of 2 K min^{-1} from 30 to 1000 °C in open alumina crucibles. Sample annealing loss was determined by a microbalance with a detection limit of 1 μg. The error is expressed as a relative error of measurement.

2.8. *In vivo evaluation of mineralized tissue formation within the DPSC-seeded CS/Gel constructs*

In this set of *in vivo* biomineralization experiments, the same experimental setting, as described for the other assays (Sections 2.6 and 2.7), was used; nevertheless, only the CS/Gel-0.1 scaffolds were further processed for the *in vivo* evaluation, based on the results obtained from the *in vitro* assays described above. This means that three experimental groups were used for the *in vivo* evaluation: 1. Cell-free scaffolds (designated as SC w/o cells) 2. DPSC-seeded scaffolds (designated as SC with cells) and DPSC-seeded scaffolds pre-incubated with rhBMP-2 for 24 h before *in vivo* transplantation (designated as SC with cells + rhBMP-2).

Before *in vivo* implantation, the DPSC/scaffold constructs were first cultured with CCM for 3 day and then medium change was performed, with or without the addition of 100 ng/ml rh-BMP-2 and incubation for another 24 h at 37 °C in 5% CO_2. Cell-free scaffolds exposed to the same conditions were used as negative controls. Cell-loaded (±rhBMP-2 pre-exposure) and cell-free scaffolds were implanted subcutaneously in the dorsum of six 6-week-old male immunocompromised mice (M/SOPF CB17/SCID, Charles River, Calco Como, Italy), applying 6 constructs per animal (total n = 36). The animals were housed in accordance with the European Community Council directive 86/609/EEC and associated guidelines (2010/63/EU) in the pathogen-free accredited animal facility of the laboratory of Anatomy, Histology & Embryology, Faculty of Veterinary Medicine, AUTH. Animals were group housed in individually ventilated cages and had *ad libitum* access to food and water. A 12 h light/dark cycle was followed. The procedures received the approval of the Veterinary Directorate of Thessaloniki (Nr. 302215/2897/26.09.2016) and the Aristotle University Ethics committee (Nr. 51/08-07-2016) and were based on the ARRIVE guidelines in full compliance with the 3Rs' rule for animals in research [27].

All animals were anesthetized after an intraperitoneal injection of a ketamine/xylazine mixture (50 and 5 mg/kg). Six subcutaneous pockets were symmetrically created in the dorsum of each animal (3/side) using blunt dissection. Each DPSC/scaffold construct (4 mm in diameter and 1–2 mm in height) was inserted into a separate pocket. Scaffolds were placed approximately 10 mm from each other in a linear fashion, dorsal to caudal, such that scaffolds were sufficiently isolated from each other and the incisions were closed with a 6-0 suture. At 6, 8 or 10 weeks following transplantation all animals were transcardially perfused with 10 ml of 0.9% saline followed by 30 ml of a 4% paraformaldehyde solution in PBS at pH 7.4 and all implants were retrieved (n = 11 for the SC w/o cells n = 14 for the SC with cells group and n = 11 for the SC with cells + rhBMP-2 group). Power analysis was used for sample size calculation, as previously described [28]. Each animal received specimens of all experimental groups (n = 6/animal).

The harvested implants were then fixed in 4% paraformaldehyde solution for an additional 24 h, routinely embedded in paraffin and cut at 10 μm with a paraffin microtome (MICROM HM315). Selected sections from each implant were then processed for histological staining (hematoxylin–eosin/H&E and Masson's trichrome staining).

The primary outcome measure was new mineralized tissue formation (evidence of osteoblast/osteocyte) confirmed by histology, SEM-EDX and XRD analysis. The observation by means of a light microscope (Zeiss, Axioplan) was blindly performed by two independent examiners. We noticed that the scaffold exhibited fluorescence in untreated sections. Therefore, for the quantification of the developed tissues (premature osteoid tissue and fully mineralized tissue) and the non-degraded scaffold, the percentage areas were measured using an Image Analysis Software (Image Pro Plus 6.3) providing the following values: a. scaffold (fluorescent in unstained sections) b. premature osteoid tissue (stained blue with Masson's) c. scaffold and fully mineralized tissue (stained red with Masson's) and d. empty space (unstained with Masson's). The percentage area occupied by fully mineralized tissue was calculated by deducting a from c.

Measurement of each scaffold's respective length and width was performed using the same Image Analysis software in H&E stained sections. Measured sections were retrieved from the same level (approximately 0.5 mm below the scaffold's surface in the transverse plane) for all scaffolds of all experimental groups in order to exclude any possible bias.

Finally, part of the retrieved specimens was processed for SEM-EDX and XRD analysis, following similar methodology, as described in Section 2.7 for the *in vitro* specimens.

2.9. Statistics

Statistical analysis of the *in vitro* and *in vivo* (histological) data employed one- or two-way ANOVA followed by Tukey's *post-hoc* test for multiple comparisons between groups (*i.e.* CS/Gel-0.1; CS/Gel-0.1 + BMP-2; CS/Gel-1; CS/Gel-1 + BMP-2). Normal distribution was confirmed by D'Agostino & Pearson normality tests. Data were expressed as means ± standard deviation (SD). For the above-mentioned analyses the Prism 6.0 Software (GraphPad, CA, USA) was used (*$p < 0.05$; **$p < 0.01$, 'n.s.' designates non-significant).

3. Results

3.1. Characterization of the CS/Gel scaffolds

The characteristic features of the fabricated CS/Gel scaffolds are summarized in Fig. 1. Two types of disc-shaped CS/Gel scaffolds were prepared for this study with a diameter of 15 mm and a height of 3 mm. The first scaffold type was crosslinked with 0.1% (v/v) GTA (CS/Gel-0.1) and the second type with 1% (v/v) (CS/Gel-1). Both scaffold types were white in colour in a dry state and, when immersed in aqueous solutions, they changed to light yellowish, with a gel-like, soft and elastic appearance. Representative SEM images showed similar porous structures for both scaffold types with interconnecting open pores and a pore size distribution in the range of 70–120 μm (Fig. 1a, b).

FTIR spectra analysis was used for the 40:60% CS/Gel scaffolds crosslinked with either 0.1% or 1% (v/v/GTA). The peaks for pure chitosan and gelatin were in accordance as previously reported [29]. For pure chitosan, the peak at 3450 cm^{-1} denotes the presence of N—H stretching, while 1654 cm^{-1} and 1580 cm^{-1} are characteristic peaks of amide I and amide II, respectively. Gelatin absorbs strongly at 3200–3500 cm^{-1}, the characteristic peak for N—H stretching and at 1640 cm^{-1} are due to C=O stretching. Both types of CS/Gel scaffolds used in the present study retained the characteristic peaks of chitosan and gelatin as shown in Fig. 1c.

Degradation analysis showed a higher degradation rate for cell-free CS/Gel-0.1 scaffolds, with a mass decrease of 48%, as compared to 18% in CS/Gel-1, at the end of the incubation period of 21 days in PBS at 37 °C, as depicted in Fig. 1d. The calculated porosity of CS/Gel-0.1 scaffolds was with 90% ± 4% higher compared to the porosity of the CS/Gel-1 counterparts, which was 83% ± 3%. The degree of swelling of CS/Gel-0.1 scaffolds indicates a value of 980% and is higher compared to CS/Gel-1, for which a value of 590% was measured.

3.2. Characterization of DPSC cultures

The DPSCs cultures used for this study expressed several MSC markers in high amounts (>90% of the population). Among those, CD146 (94.5 ± 4.1%), CD90/Thy-1 (99.4 ± 0.4%), CD73 (98.4 ± 1.9%), CD49f/a6-integrin (95.2 ± 2.4%), nestin (97.7 ± 2.5%) and CD105 (91.5 ± 4.8). Lower expression was observed for STRO-1 (12.7 ± 4.8%), CD106 (47.6 ± 6.6%) and the embryonic SC markers SSEA-1 (2.9 ± 0.8%), SSEA-3 (8.3 ± 2.6%), SSEA-4 (51.4 ± 7.9%), Nanog (72.6 ± 8.0%) and Oct3/4 (10.3 ± 3.5%). Finally, the hematopoietic stem cell markers showed minor expression, as for CD34 (2.3 ± 0.7%) or were not expressed at all (CD45 and CD117 < 1%) (Fig. 2).

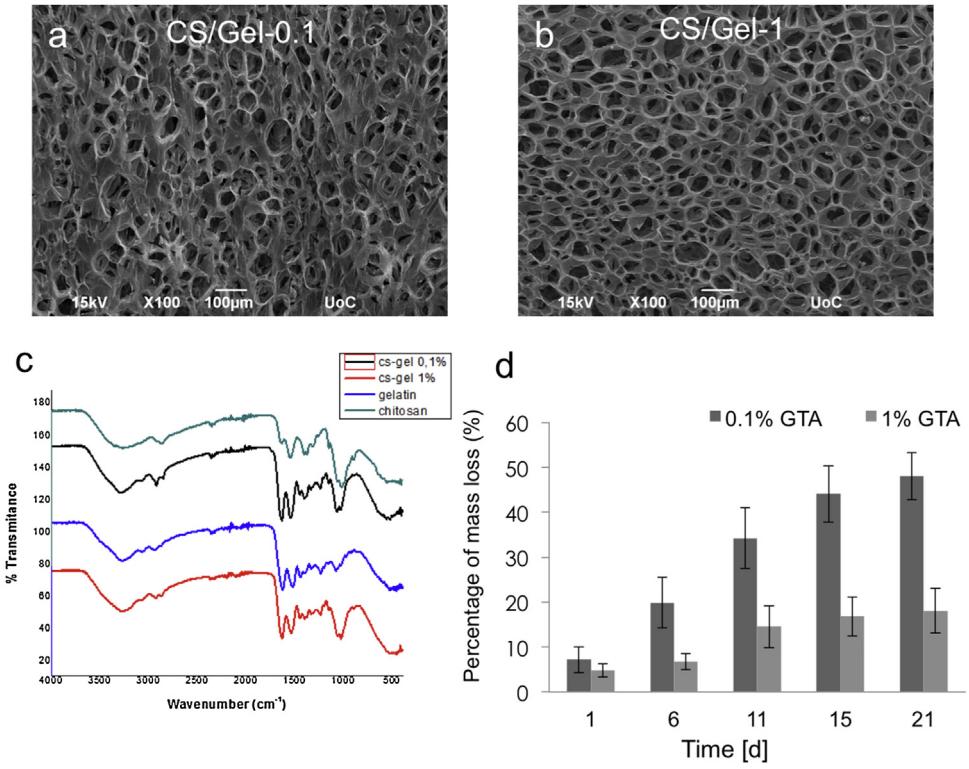

Fig. 1 – Characterization of fabricated CS/Gel scaffolds crosslinked either with 0.1% (v/v) (CS/Gel-0.1) or with 1% (v/v) (CS/Gel-1) glutaraldehyde (GTA). (a, b) Representative SEM images showing the structure of both scaffold types with interconnecting pores and a pore size in the range of 70–120 μm. (c) Representative FTIR spectra. (d) Degradation graph. Results are means of three independent experiments (N = 3) in three technical replicates each (n = 3).

3.3. *Assessment of cell morphology and viability/proliferation of DPSCs inside the CS/Gel scaffolds*

A successful adhesion and spreading inside the highly porous structure of both scaffold types (CS/Gel-0.1 and CS/Gel-1) was confirmed by SEM observation to occur as early as 24 h after seeding. Cells showed a typical spindle-shaped morphology with multiple extensions and filopodia, as shown in Fig. 3A (a–d).

A statistically significant ($p < 0.01$ for both scaffold types), time-dependent increase of DPSC mitochondrial dehydrogenase activity-commonly used as an indirect marker of cell viability/proliferation- inside the constructs from day 1 to day 7 was shown by the MTT assay. This initial increase was, however, followed by statistically significant reduction ($p < 0.05$ for both scaffold types) at day 14, possibly attributed to the initiation of differentiation phenomena inside the constructs (Fig. 3B). Notably, there was a statistically significant higher cell viability of DPSCs inside the CS/Gel-0.1, as compared to the CS/Gel-1 scaffolds during the first three days after cell seeding ($p < 0.05$), while differences in cell viability were compensated to non-significant at later time-points (day 7, day 14).

Live/dead fluorescent staining showed that that more than 90% of the cell population remained viable throughout the observation time (up to day 14), as they appeared green by the enzymatic digestion of the fluorescent dye calcein AM, while very few dead cells (not exceeding 5–10% in all cases) were stained red from the EthD1 that was incorporated into to their nuclei after passing though the damaged membranes (Fig. 3C (a–f)). Noteworthy, there was an even distribution of the cells inside the entire porous structure of the scaffolds, leading to full coverage of their pores, which suggests a successful spreading and growth of the initially seeded cell population. In full accordance with the MTT data, CS/Gel-0.1 scaffolds contained more cells at day 3 compared to the CS/Gel-1 scaffolds, whereas no differences could be observed at day 7 and day 14.

3.4. *Assessment of expression of osteo/odontogenic differentiation genes by DPSCs inside the CS/Gel scaffolds*

Expression of several osteo/odontogenic differentiation markers was comparatively analyzed for DPSCs cultured inside CS/Gel-0.1 and CS/Gel-1 scaffolds, with or without previous single pre-exposure to rhBMP-2 (100 ng/ml, 24 h). Differential gene expression patterns could be observed in the four experimental groups (*i.e.* CS/Gel-0.1; CS/Gel-0.1 + rhBMP-2; CS/Gel-1; and CS/Gel–1 + rhBMP-2) at different time points (day 7 and day 14). The results are presented in Fig. 4a–f.

In specific, incubation of DPSCs inside the CS/Gel-0.1 scaffolds was effective to induce a statistically significantly upregulation of all osteo/odontogenic markers, including *DSPP* (day 7, day 14), *IBSP* (day 7, day 14), *Osterix* (day 7, day 14), *BMP-2* (day 7, day 14), *BGLAP* (day 7, day 14) and *ALP* (day 7). This was evident in both non-induced (CS/Gel-0.1), as well

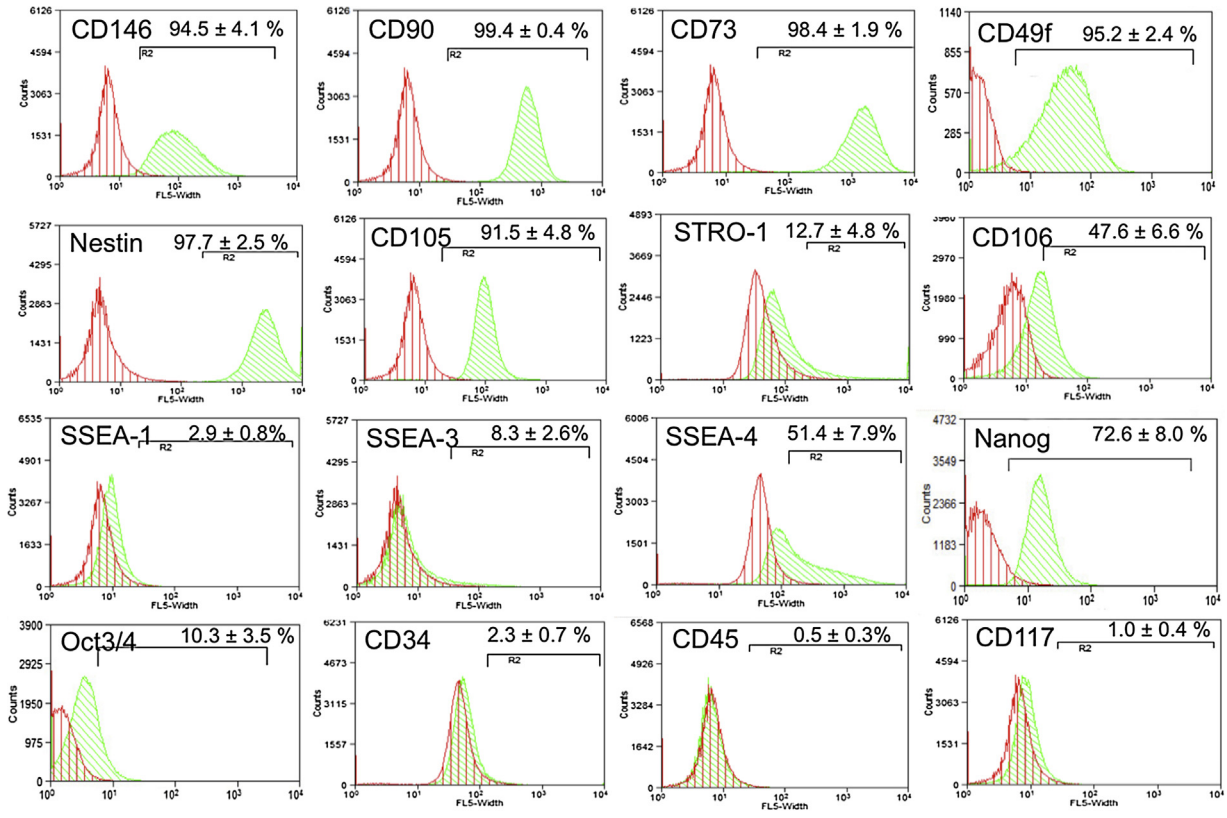

Fig. 2 – Representative flow cytometry histograms showin the immunophenotypic characterization results of DPSC cultures for the expression of mesenchymal (CD146/MUC18, CD90/Thy-1, CD73, CD49f/a6-integrin, nestin, CD105/endoglin, STRO-1, CD106), embryonic (SSEA-1, SSEA-3, SSEA-4, Nanog, Oct3/4) and hematopoietic (CD34, CD45, CD117/c-kit) stem cell markers (green line: unstained control, red line: marker of interest). Results are means of the expression of three different cell donors, with experiments were run three times for each donor (N = 3) in two technical replicates each (n = 2). (For interpretation of the references to colour in this figure legend, the reader is referred to the web version of this article.)

as pre-induced (CS/Gel-0.1 + rhBMP-2) constructs. However, significant differences were observed after performing multiple comparisons between CS/Gel-0.1 and CS/Gel-0.1 + rhBMP2 constructs: at day 7 the upregulation of all six markers was significantly higher in CS/Gel-0.1, as compared to CS/Gel-0.1 + rhBMP-2 constructs ($p < 0.01$ in all cases), while at day 14 the expression was significantly higher for *DSPP*, *ISBP* and *Osterix* for the CS/Gel-0.1 – ($p < 0.05$ for *DSPP* and *IBSP* and $p < 0.01$ for *Osterix*) and for *BMP-2*, *BGLAP* and *ALP* for the CS/Gel-0.1 + rhBMP-2 constructs ($p < 0.01$).

In contrast, the gene expression patterns were quite different for the DPSCs incubated inside the CS/Gel-1 scaffolds. In more detail, a statistically significant upregulation of *BMP-2* (day 7, day 14), *BGLAP* (day 7, day 14) and *ALP* (day 7, day 14), but not *DSPP*, *IBSP* (at any time-point) and *Osterix* (upregulation observed only for the CS/Gel-1 + rhBMP2 constructs at day 7) was triggered inside both CS/Gel-1 and CS/Gel-1 + rhBMP2 constructs; while multiple comparisons (CS/Gel-1 *vs.* CS/Gel-1 + rhBMP2) showed that at day 7 the upregulation of *BMP-2*, *DSPP* and *ALP* was significantly higher in the non-induced, as compared to the pre-induced constructs ($p < 0.01$ for *BMP-2* and $p < 0.05$ for *DSPP* and *ALP*), while at day 14 the expression was significantly higher for *BMP-2* in the pre-induced constructs ($p < 0.01$), and for *ALP* in the non-induced constructs ($p < 0.0$-).

Overall, the *in vitro* experiments could not confirm any exceptional impact of the rhBMP-2 pre-exposure on the upregulation of the expression of osteo/odontogenesis-related markers in either type of scaffolds.

3.5. *Characterization of the mineralized tissue produced inside the DPSC-seeded CS/Gel scaffolds*

SEM-EDX analysis of the DPSC-seeded CS/Gel scaffolds after 4 and 8 weeks incubation in phosphate-rich CCM showed abundant CaP phase-rich tissue that was newly generated inside the scaffolds to overspread their entire structure (Fig. 5). This was evident in all four experimental groups (*i.e.* CS/Gel-0.1; CS/Gel-0.1 + rhBMP-2; CS/Gel-1; and CS/Gel-1 + rhBMP-2) at both time points [4 weeks, data not shown and 8 weeks, Fig. 5a–f and g–l]. DPSC bodies were partially covered and embedded within the cell-produced mineralized matrix. In contrast, only sparse precipitation of calcified tissue (CaP phase) could be detected in the cell-free scaffolds (Fig. 5a, g), therefore excluding spontaneous mineral precipitation attributed to culture medium hypersaturation. EDX-based calculation of the calcium (Ca) to phosphorus (P) ratio showed that it was in the range of 1.3–1.4 for all DPSC/scaffold constructs (Fig. 5b, h), which is close to the ratio in biological

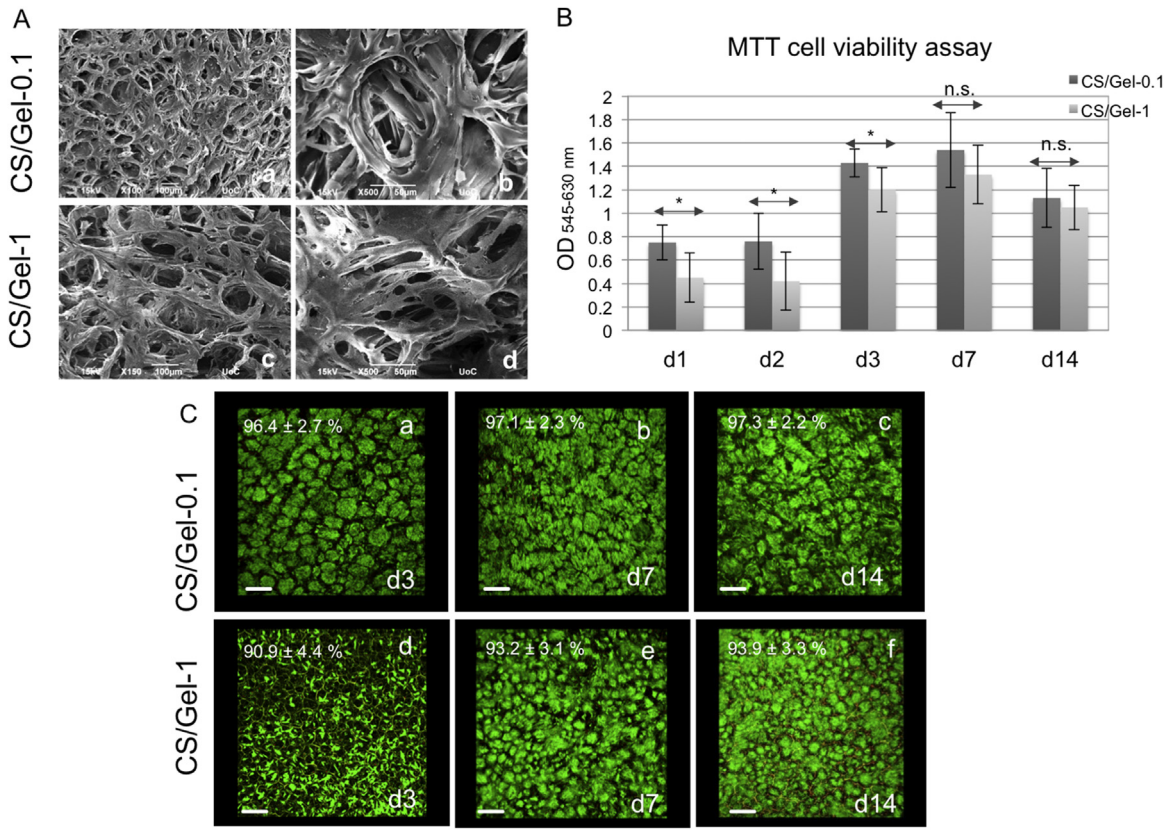

Fig. 3 – Evaluation of cell attachment and viability/proliferation of DPSCs inside the CS/Gel constructs. (A) Representative SEM images showing successful initial adhesion and spreading of DPCSs inside the CS/Gel-0.1 (a, b) and CS/Gel-1 (c, d) scaffolds 24 h post-seeding. (B) MTT cell viability/proliferation assay of DPSC-seeded CS/Gel-0.1 and CS/Gel-1 scaffolds after 1, 2, 3, 7 and 14 days. The optical density (OD) was measured at 545 nm with a reference filter at 630 nm. Data represent the average (±SD) of DPSC cultures established from three donors, with experiments run three times for each donor (N = 3) with three technical replicates each (n = 3). (C) Live/dead fluorescent staining with calcein AM/ethidium homodimer and representative confocal microscopy images of DPSC-seeded CS/Gel-0.1 (a–c) and CS/Gel-1 (d–f) scaffolds after 3, 7 and 14 days in culture. High levels of cell viability with very few dead cells (<5 to 10%) could be observed for both scaffolds at all time-points. CS/Gel-0.1 scaffolds contained more cells at day 3 compared to CS/Gel-1 scaffolds, while no differences could be observed at day 7 and day 14. Note: the percentages over each photo show the average (±SD) of living cells of DPSC cultures established from three donors, with experiments run three times for each donor (N = 3) in two technical replicates each (n = 2). (For interpretation of the references to colour in the text, the reader is referred to the web version of this article.)

apatite (1.7). The Ca to P ratio was not calculated for the cell-free scaffolds due to the very low amounts of both elements in these experimental groups (Fig. 5a, g).

XRD analysis confirmed the apatitic nature of the newly formed mineralized tissues, as evidenced by the presence of a nano-crystalline CaP phase corresponding to the characteristic peak around 32 (2θ) in the respective diffractograms of cell-loaded constructs; something not present in the cell-fee scaffolds (Fig. 6a–f). This peak was quite low at the 4 weeks samples (data not shown), but clearly evident in all cell-seeded 8 weeks samples (CS/Gel-0.1; CS/Gel-0.1 + rhBMP2, CS/Gel-1; and CS/Gel–1 + rhBMP2). Rietveld refinement provided further information on the lattice parameters that indicated the building of biological apatite in all DPSC/scaffold constructs with a crystallite size of 9–10 nm (Fig. 6g).

Quantification of the inorganic content inside the constructs by ashing the sample in an oxygen atmosphere showed that a higher mineral content was observed inside the CS/Gel-0.1 + rhBMP-2 (15.3 ± 0.2%), as compared to the CS/Gel-0.1 (9.5 ± 0.4%), while no major differences could be observed between the CS/Gel-1 (12.7 ± 0.2%) and the CS/Gel–1 + rhBMP-2 (11.9 ± 0.3%) scaffolds (Table 2).

3.6. *In vivo regeneration of mineralized bone-like tissues within the DPSC-seeded CS/Gel constructs*

The cell-free and cell-loaded (±rhBMP-2) constructs were subcutaneously implanted into SCID mice for 6–10 weeks to test the capability of generating mineralized, bone-like tissues *in vivo*. As shown in the histological sections stained with H & E and Masson's trichrome respectively (Fig. 7A (a–i) and B (a–i)), abundant ECM and mineralized tissue were generated inside all three experimental groups by 6 weeks following subcutaneous implantation and were maintained (cell-free scaffolds)

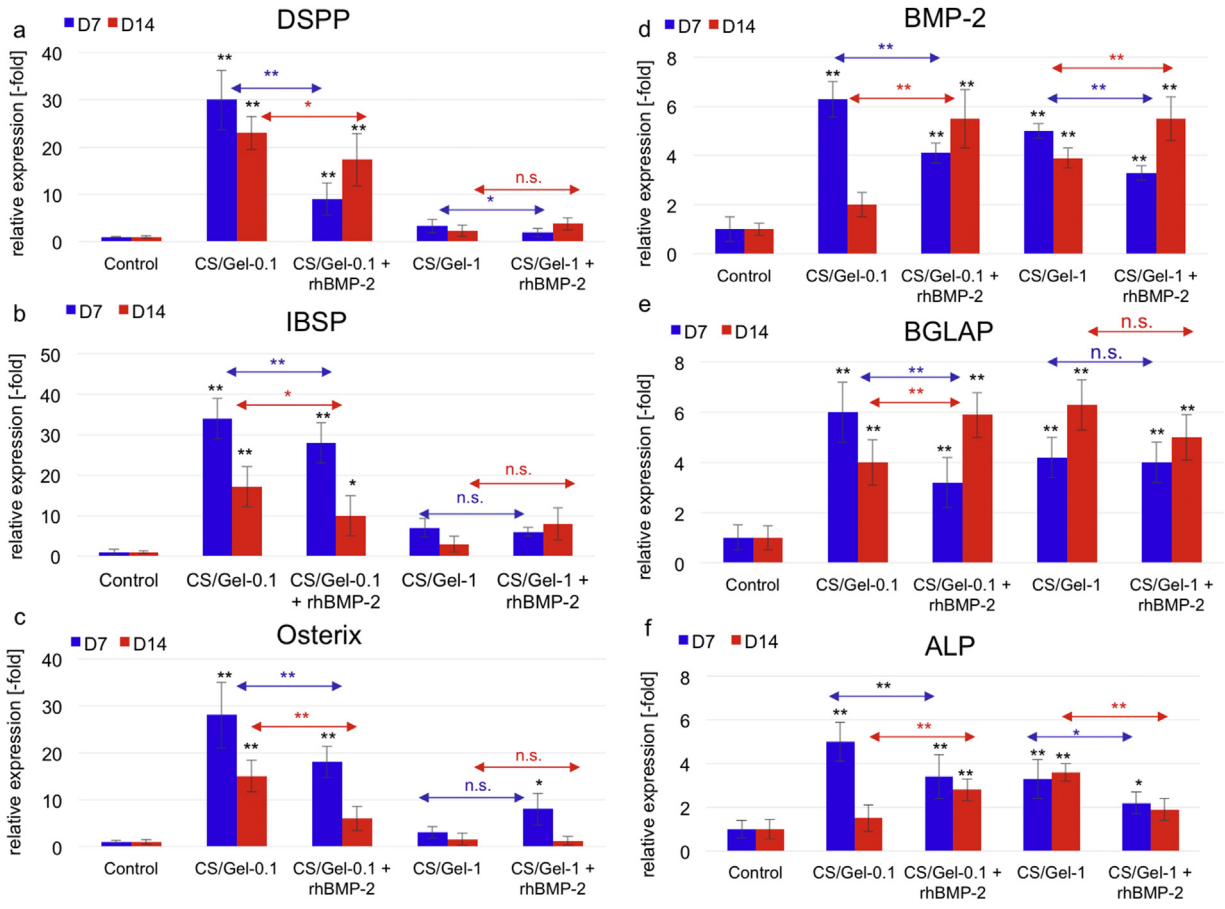

Fig. 4 – Real-time PCR analysis of the expression of osteo/odontogenic markers including (a) *DSPP*, (b) *IBSP*, (c) *Osterix*, (d) *BMP-2* (e) *BGLAP* and (f) *ALP* in DPSC-seeded CS/Gel-0.1 and CS/Gel-1 scaffolds after 7 and 14 days, with/without additional single pre-exposure to 100 ng/ml (for 24 h) rhBMP-2. Values are means (±SD) of DPSC cultures established from three donors, with experiments run three times for each donor (N = 3) in two technical replicates each (n = 2). Asterisks indicate statistically significant differences between each experimental group (*i.e.* CS/Gel-0.1; CS/Gel-0.1 + rhBMP-2; CS/Gel-1; and CS/Gel-1 + rhBMP-2) compared to the baseline expression (control). Asterisks over blue and red double arrows indicate statistically significant differences between non-induced and rhBMP-2 pre-induced scaffolds at day 7 (blue arrows) or at day 14 (red arrows). SDHA and B2M were used as housekeeping controls (*$p < 0.05$; **$p < 0.01$, n.s. designates non-significant). (For interpretation of the references to colour in this figure legend, the reader is referred to the web version of this article.)

or increased (cell-loaded scaffolds) up to 10 weeks. H&E staining showed clear cell infiltration, uniform cell distribution and the homogenous deposition of ECM throughout all constructs (Fig. 7A (a–i)). New bone formation was observed in all experimental groups (*i.e.* SC w/o cells; SC with cells; and SC with cells + rhBMP-2) but was clearly more evident in those that were pre-exposed to rhBMP-2 for 24 h in culture before implantation. Masson's trichrome staining further showed that the premature osteoid tissue rich in collagen I (stained blue) was gradually replaced by fully mineralized tissue (stained red), with osteocytes entrapped within the lacunae and lamellae; On the other hand, empty areas, as well as non-degraded scaffold were still visible inside the constructs even after 10 w *in situ* (Fig. 7B (a–i)).

Quantitative analysis of the regenerated mineralized tissues inside the constructs indicated that, at 6 weeks after implantation, a statistically significantly higher amount of osteoid ($p < 0.01$), as well as fully mineralized bone ($p < 0.01$) could be observed in rhBMP-2 pre-induced constructs compared to the other two groups. However, the amount of bone was significantly higher for the cell-free compared to the cell-loaded scaffolds that were not pre-exposed to rhBMP-2. Moreover, the rhBMP-2 pre-induced scaffolds, showed a significantly lower amount of empty space, but also a higher amount of remaining (non-degraded) scaffold at 6 weeks, compared to the other two groups (Fig. 8a). The same profile was maintained at 8 weeks, with further increase in osteoid tissue only in rhBMP-2 pre-induced constructs (SC w/o cells < SC with cells < SC with cells + rhBMP-2; $p < 0.01$); while the amount of mineralized bone was similar in all three experimental groups. The amount of empty space was lower in the rhBMP-2 pre-induced constructs (as at 6 weeks), while the amount of non-degraded scaffolds was the highest in the cell-free scaffolds (Fig. 8b). Finally, at 10 weeks after implantation, osteoid

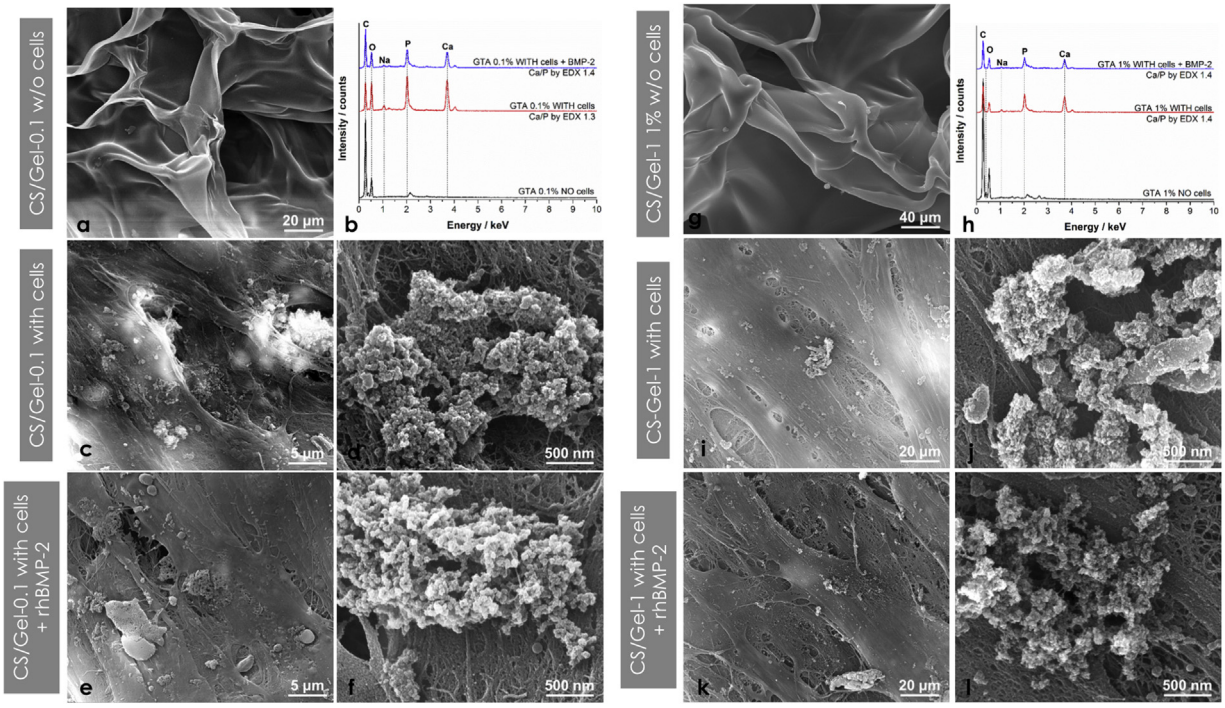

Fig. 5 – Representative SEM images of cell-free (a) DPSC-seeded (c, d) and DPSC-seeded + rhBMP-2 (e, f) CS/Gel-0.1 scaffolds after 8 weeks in culture; respective images for cell-free (g) DPSC-seeded (i, j) and DPSC-seeded + rhBMP-2 (k, l) CS/Gel-1 scaffolds. Abundant newly-formed, nanocrystalline CaP mineralized tissue was generated within the cell-seeded scaffolds of all experimental groups, with cell bodies being entrapped within the secreted matrix. In contrast, only sparse precipitation of calcified tissue could be detected in the cell-free scaffolds. Representative EDX spectra-based calculation of the calcium (Ca) to phosphorus (P) ratio of CS/Gel-0.1 (b) and CS/Gel-1 (h) scaffolds showed that it was in the range of 1.3–1.4 for all cell-seeded constructs.

tissue had further matured into fully mineralized bone in all groups, with an obviously higher amount in rhBMP-2 pre-induced constructs compared to the other groups (SC w/o cells < SC with cells < SC with cells + rhBMP-2; $p < 0.01$) (Fig. 8c). The same profile regarding empty space/non-degraded scaffold was observed at this time-point, as with the 6 and 8 weeks results.

Measurement of the length (Fig. 8d) and width (Fig. 8e) of the histological sections of all constructs showed that the cell-free constructs exhibited a slower initial degradation rate, as evidenced by a significantly lower reduction of their length until 8 weeks ($p < 0.05$), as compared to the cell-loaded scaffolds (both with or w/o rhBMP-2 induction). However, the deterioration of the cell-free scaffolds was accelerated at 10 weeks, in contrast to the cell-loaded constructs that gradually started to increase in size due to becoming filled with abundant, newly-formed ECM (Fig. 8d). With respect to construct width, a slower initial reduction rate was observed for the rhBMP-2 pre-induced constructs (6 weeks; $p < 0.05$) but differences were compensated at later time-points for all three experimental groups, showing no statistical significance (Fig. 8e).

SEM images of the retrieved constructs after 10 weeks *in situ* showed formation of mineralized precipitates, consisting of spherical nanosized particles with a minimum size of 50 nm (Fig. 8f, g). In both cases the calcium (Ca) to phosphorus (P) ratio was close to 1, as determined by EDX (Fig. 8h, i). This could be attributed to the substituted biological apatite with incorporated sodium (Na) and magnesium (Mg) ions, correspondingly decreasing the Ca to P ratio. It is important to mention that the size of the apatite particles formed was similar for *in vitro* and *in vivo* samples.

4. Discussion

Several types of biomaterials have been extensively employed for bone TE, namely natural biomaterials [13,29], synthetic polymers, hybrids [30], ceramic materials [31] including bioactive glasses [32] and composites [33]. Among these, chitosan-based natural biomaterials have attracted particular attention for application in bone TE due to their excellent biocompatibility and their ability both to maintain cell viability/proliferation while promoting osteogenic differentiation of a variety of cell types [34]. Other important advantages include their antimicrobial activity, which is crucial for oral applications [35] – combined with ease of production and the ability to tune their mechanical and biological properties. This can be achieved mainly by varying the type and concentration of the crosslinking agents used for blending chitosan with other natural biomolecules, such as for *e.g.* collagen or gelatin interacting with the available chemical groups of chitosan. In the present study, biomimetic CS/Gel natural polymers [10] (Fig. 1) were employed as scaffolds for hosting dental MSCs

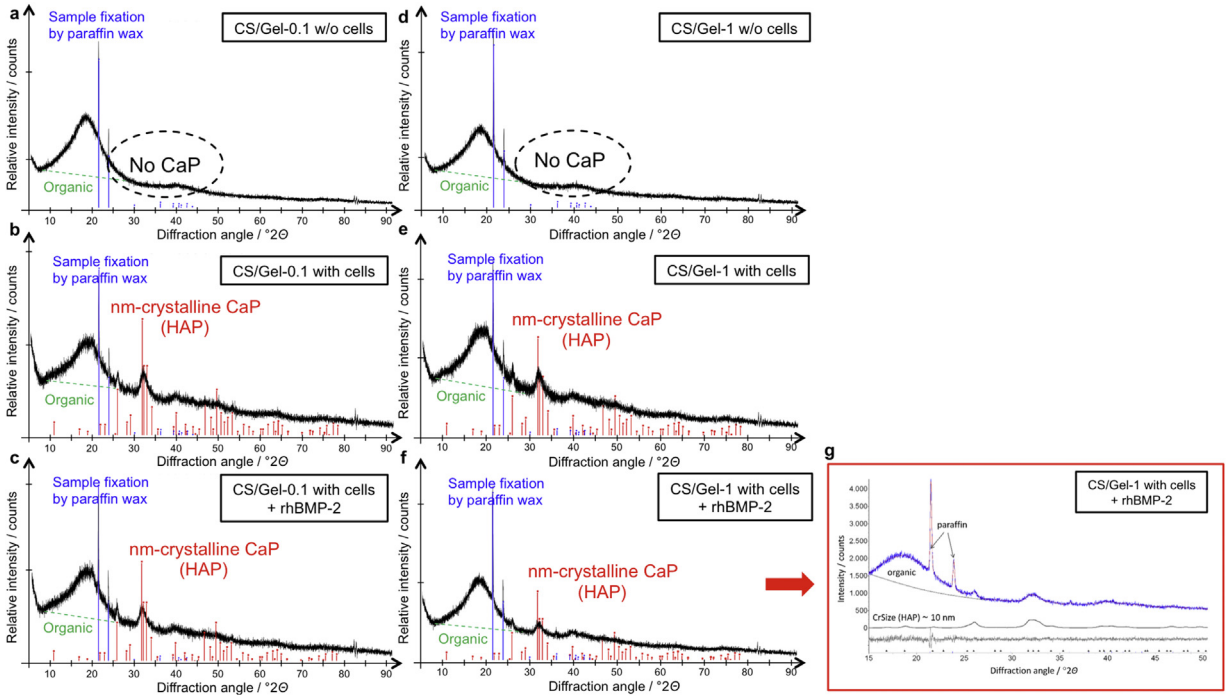

Fig. 6 – Representative XRD diffractograms of cell-free (a) DPSC-seeded (b) and DPSC-seeded + rhBMP-2 (c) CS/Gel-0.1 scaffolds after 8 weeks in culture; respective XRD diffractograms for cell-free (d) DPSC-seeded (e) and DPSC-seeded + rhBMP-2 (f) CS/Gel-1 scaffolds. The formation of biological apatite is verified by the characteristic peak around 32° (2θ). Representative diffractogram of the Rietveld analysis performed to calculate lattice parameters of the crystalline phase (crystalline size of 9–10 nm) (g).

Table 2 – Calculation of the inorganic content (%) of the different types of experimental constructs by means of thermogravimetry (TG).

Sample	Inorganic content (% ± SE)
CS/Gel 0.1% w/o cells	Not detectable
CS/Gel 0.1% with cells	9.5 ± 0.4
CS/Gel 0.1% with cells + rhBMP-2	15.3 ± 0.2
CS/Gel 1% w/o cells	2.5 ± 0.5
CS/Gel 1% with cells	12.7 ± 0.2
CS/Gel 1% with cells + rhBMP-2	11.9 ± 0.3

(DPSCs) (Fig. 2) in a comprehensive translational *in vitro/in vivo* approach targeting craniofacial bone regeneration. The study was inspired by the clinical data of two randomized controlled clinical studies conducted by our group using autologous BM-MSCs combined with commercially available collagen scaffolds for the regenerative treatment of intrabony periodontal defects (*ClinicalTrials.gov ID: NCT02449005*) together with the preservation of peri-implant bone (*ClinicalTrials.gov ID: NCT03070275*). We aimed to produce novel, optimized TE constructs using natural biomaterial scaffolds, with ease to handle and shape them to meet the specific needs of alveolar bone regeneration.

Mimicking osteogenic ECM is an important component of any strategy in preparing biomimetic scaffolds for bone TE. Chitosan has both a structural similarity to the ECM of bone tissue and inherent immune-stimulating properties; these properties, both conducive to local healing processes, make it a prime candidate for use in bone TE. Bone healing necessitates a chain of events that follow an initial disruption of bone architecture. These events include the initiation of an inflammatory response orchestrated by the activation of macrophages and recruitment of platelets. These in turn attract – through their paracrine activity and release of various cytokines – other cells [36], including osteoprogenitor cells, osteoblasts and endothelial cells to form new blood vessels. Given the importance of these processes not being disturbed by the presence of foreign bodies, natural ECM-mimicking biomaterials, including chitosan and gelatin, offer significant advantages compared to alternatives, such as synthetic polymers, hybrids or ceramics.

Other important parameters directly affecting biological properties include scaffold architecture, porosity, pore size and pore interconnectivity. In the present study, chemical crosslinking of the two scaffold types combined with the freeze-drying technique led to the fabrication of scaffolds with a controlled pore size in the range of 70–120 μm, which has been proven beneficial to promoting adhesion and proliferation of various MSC types compared to higher pore sizes [37]. The high porosity of 83–90% with interconnected channels allowing cells to migrate into the 3D structure to obtain nutrition from the culture medium has been also reported to favour bone TE [38,39]. The existence of interconnected pores is also of critical importance to promote neovascularization while preventing necrotic tissue formation at the core of the scaffold [40]. The high swelling ratios after 30 min of immersion in water indicate that both scaffold types take up water that is much more than their own weight, with the CS/Gel-0.1 scaf-

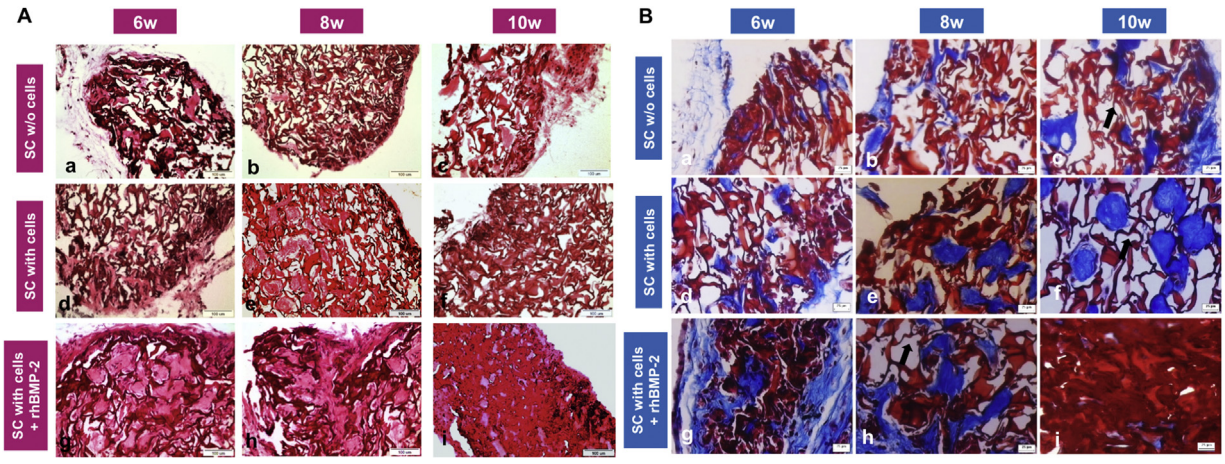

Fig. 7 – A H&E staining of cell-free (a–c), DPSC-loaded (d–f) and DPSC-loaded + rhBMP-2 (24 h pre-induction with 100 ng/ml rhBMP-2 for 24 h before *in vivo* transplantation) (g–i) CS/Gel-0.1 scaffolds after 6–10 weeks *in situ* into the dorsum of immunocompromised mice; New bone formation was observed in all experimental groups, but was clearly more evident in those that were pre-exposed to rhBMP-2. B Masson's trichrome staining of cell-free (a–c), DPSC-loaded (d–f) and DPSC-loaded + rhBMP-2 (g–i) CS/Gel-0.1 scaffolds after 6–10 weeks *in situ*. Osteoid tissue rich in collagen I (stained blue) was gradually replaced by fully mineralized tissue (stained red), with osteocytes entrapped within the lacunae and lamellae; the latter being more evident in constructs pre-exposed to rhBMP-2, followed by the cell-loaded constructs (without pre-exposure), while it was less obvious in cell-free constructs. Areas of non-degraded scaffold could be also visible inside all constructs (black arrows). (For interpretation of the references to colour in this figure legend, the reader is referred to the web version of this article.)

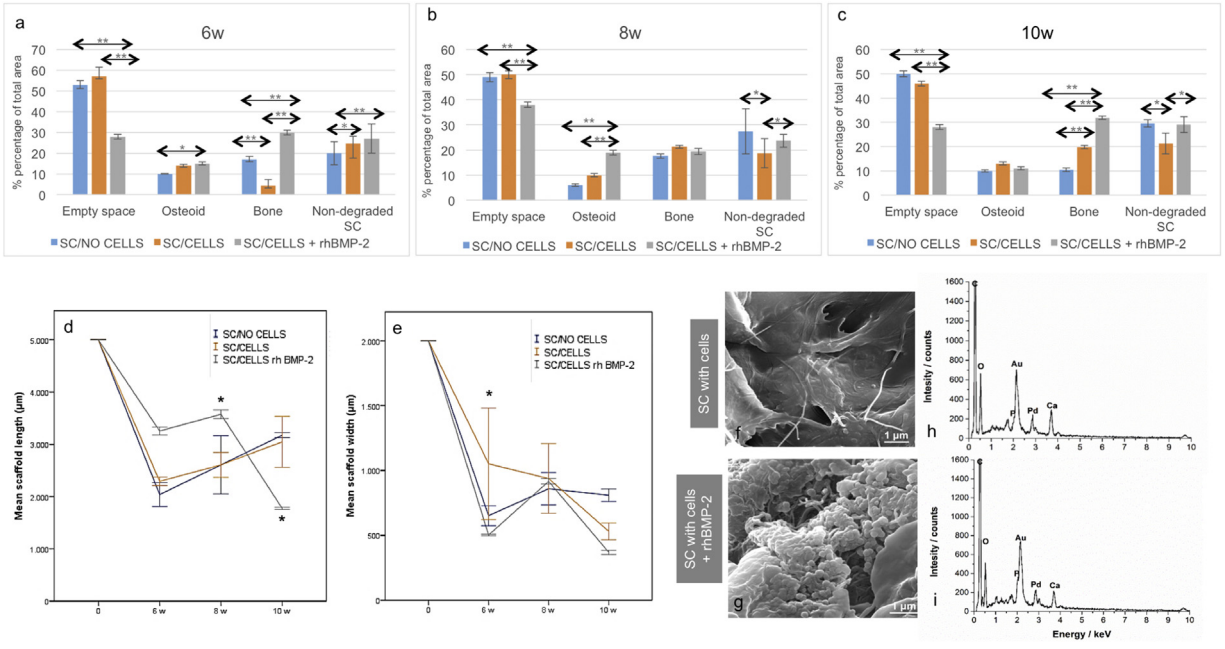

Fig. 8 – Bar diagrams showing the quantification of the empty space, osteoid, bone and non-degraded scaffold in all three experimental groups (SC/NO CELLS; SC/CELLS; SC/CELLS + rhBMP-2) after 6 (a), 8 (b), and 10 (c) w *in situ*. Values are means (±SD) of each construct in 3–4 replicates for each experimental group and time-point. Asterisks over double arrows indicate statistically significant differences between groups (*$p < 0.05$; **$p < 0.01$). Line diagrams of the length (d) and width (e) of the constructs, as measured in histological sections of specimens retrieved after 6–10 weeks. SEM images of the SC/CELLS (f) and SC/CELLS + rhBMP-2 (g) constructs, retrieved after 10 weeks *in situ*, confirming the formation of nanocrystalline CaP particles, similar to the *in vitro* specimens. Representative EDX spectra of the SC/CELLS (h) and SC/CELLS + rhBMP-2 (i) constructs showed a Ca to P ratio of approx. 1.

fold type presenting a higher swelling ratio value, which may be attributed to the higher distance between the bonds in the network of this hydrogel. This is a desired property as it leads to pore size enlargement and facilitates cell attachment and growth in three dimensions [29,41]. The rheological properties of both scaffold types as observed by dynamic storage modulus values of 3 and 7 kPa, respectively, are characteristic for strong hydrogels (data not shown). Both scaffold types showed immediate structure recovery as the imposed strain amplitude decreased to linear regime values. Additionally, temperature variation from 25 to 37 °C did not affect their viscoelastic properties.

A drawback of chitosan is the lack of adhesion motifs to support direct cell anchorage. Previous studies have shown that several MSC types, such as adipose tissue-derived MSCs [42] and human umbilical cord MSCs [43] have an inability to spread and proliferate on chitosan films or membranes attributed to the activation of cell signalling pathways affecting cellular mobility by chitosan chemical cues [44]. A recent study [45] reports on the functionalization of chitosan scaffolds with either RGD sequences or fibronectin molecules to address poor initial DPSC attachment in contact with non-functionalized chitosan. However, even the functionalized scaffolds failed to trigger DPSC osteo/odontogenic differentiation, leaving a lacuna in the development of optimal properties to trigger mineralized tissue regeneration in chitosan-based biomimetic matrices.

This prompted us in the present study to blend chitosan with gelatin, a natural biomolecule containing RGD and the most common cell-binding peptide found in cell adhesion proteins, such as fibronectin and laminin [46]. In contrast to physical crosslinking methods, such as dehydrothermal treatment, plasma method and irradiation-based techniques, which, although safe and inexpensive, may lead to the surface leakage of proteins and an overall inferior degree of crosslinking, chemical crosslinking can provide an irreversible and longer-term functional stability [47]. Commonly used chemical crosslinking agents include aldehydes such as formaldehyde, glutaraldehyde, glyceraldehyde, glyoxal, polyepoxy compounds, carbodiimides [47] and natural crosslinking agents, such as genipin [9]. Chemical crosslinking has proven beneficial in maximizing the mechanical properties of bone substitutes; however, most reagents used for this purpose exhibit adverse effects and may trigger toxic reactions. In a recent study of our group [12], CS/Gel scaffolds with the same composition (40:60) as in the present study were fabricated by lyophilization and chemically crosslinked with either 0.1% (v/v) glutaraldehyde (GTA) or 0.1% (v/v) genipin before evaluation for adhesion, proliferation and differentiation properties of pre-osteoblastic cells and human BM-MSCs. The results showed a strong cell infiltration of pre-osteoblasts into the pores of GTA-crosslinked scaffolds compared to the genipin-crosslinked counterparts. Taking into account the cost-efficiency of GTA *vs.* genipin and the undesirable blue colour of the latter, we decided to investigate GTA-crosslinked scaffolds in the present study.

GTA has been extensively employed as a gold standard in crosslinking tissue films and scaffolds, providing the maximum possible degree of crosslinking resulting in superior mechanical properties [47]. GTA reacts with the free amine groups of lysine or hydroxylysine amino acid residues in the gelatin polypeptide chains to produce imine linkages forming an interpenetrating network [48]. Although this poses the risk of GTA-induced toxicity, this can be eliminated by controlling the crosslinker concentration in the solution and/or by an efficient extraction of unreacted GTA that remains in the material after the crosslinking treatment [49]. GTA concentrations in polymeric solutions up to 5% (wt%) have been shown not to be cytotoxic in mammalian cells [50]. In accordance with these findings, the results of the present study showed the viability and attachment properties of DPSCs were maintained in both CS/Gel-0.1 and CS/Gel-1 scaffolds (Fig. 3A), although a lower viability/proliferation rate (Fig. 3B) and cell density (Fig. 3C) could be observed in the scaffolds with the highest GTA concentration during the first three days in culture that was eliminated at later time-points. Despite the lack of initial signs of cytotoxicity, major differences were observed in the osteo/odontogenic differentiation potential of DPSCs after increasing the crosslinking agent concentration from 0.1 to 1% (Fig. 4). Indeed, DPSCs seeded in CS/Gel-1 scaffolds did not show upregulation of three (*DSPP*, *IBSP* and *Osterix*) out of six differentiation markers (*BMP-2*, *BGLAP*, *ALP*, *DSPP*, *IBSP* and *Osterix*) implying a long-term cytotoxic effect of GTA at concentrations seemingly initially non-toxic when viability is considered as the biological endpoint. These results indicate that even a minor increase in the crosslinker concentration at sub-toxic levels may impact severely on the biological properties, which are highly important for bone TE. Overall, these results confirm the first research hypothesis of this study. In consensus with this study, other studies have shown that the osteogenic potential of chitosan hydrogels can be tuned by altering the concentration of the chemical crosslinker [10].

The rationale for choosing to evaluate scaffolds crosslinked at two different GTA concentrations was based on the degradation analysis data of the cell-free scaffolds (Fig. 1d), showing a mass decrease of 48% in CS/Gel-0.1 scaffolds as compared to only 18% in CS/Gel-1 after 21 days. Since initial bone healing in alveolar defects usually takes 6 weeks [51,52], it is desirable to use scaffolds able to support initial healing processes before being replaced by local bone tissue. Despite the higher degradation rate of the cell-free CS/Gel-0.1 scaffolds, both types of cell-loaded scaffolds favoured abundant ECM production and subsequent extensive mineralization by DPSCs after 4 weeks in culture, together with nanocrystalline hydroxyapatite formation after 8 weeks (Figs. 5 and 6). TG analysis confirmed similar amounts of inorganic content in both scaffolds types (CS/Gel-0.1; CS/Gel-1) (Table 2).

Further characterization of the nature of mineralized tissue by means of XRD and Rietveld analysis of the lattice parameters showed that at the end of 4 weeks *in vitro* only a minor peak around 32° (2θ) corresponding to biological apatite could be detected (data not shown); this was, however, clearly evident after 8 weeks (Fig. 6) confirming the crystalline nature of the mineralized ECM. EDX-based calculation of the Ca to P ratios (approx. 1.3–1.4) (Fig. 5b, h) and Rietveld analysis of the lattice parameters detecting a crystalline size of 9–10 nm (Fig. 6g) confirmed the successful formation of biological apatite within all the cell/scaffold constructs. In agreement with this study, a previous study [40] on chitosan-based hydrogel scaffolds made by 3D plotting showed that differentiation

into osteocytes is gradually achieved by a sequence of events that include abundant secretion of collagen-I during the first week, followed by upregulation of alkaline phosphatase activity, that in turn initiates the biomineralization process by facilitating formation and nucleation of CaP. The most important observation in this study is that biological apatite formation could be achieved simply by seeding DPSCs in the biomimetic matrices, even in the samples not externally triggered by rhBMP-2. In most other studies, coating or dispersion of (nano)hydroxyapatite particles in chitosan-based matrices was an important prerequisite for achieving *in vitro* [53] and *in vivo* biomineralization [54]. In order to exclude the possibility of the detected hydroxyapatite being a product of the precipitation commonly occurring in various biologic solutions, such as simulated body fluid (SBF) [55] or other supersaturated solutions, such as the phosphate-rich a-MEM medium used in the present study, cell-free scaffolds were also equally exposed to the same conditions. The SEM-EDX and XRD data confirmed only minor CaP precipitation even after 8 weeks in culture, confirming that the nanocrystalline CaP tissue detected in cell-loaded constructs was a product of *in vitro* biomineralization of the abundantly secreted ECM matrix.

Several growth factors have been extensively applied to promote osteogenesis. Among those members of the transforming growth factor-beta superfamily, including BMP-2, BMP-3 (osteogenin), BMP-4 and BMP-7 (osteogenic protein-1) are the most widely used. BMP-2 and BMP-4 have been found to have a role in developing tooth buds, the odontoblastic layer and craniofacial bones (intramembranous ossification), while other members of the BMP family, such as BMP-3 and BMP-7, are mainly involved in endochondral bone formation procedures [56]. Previous studies have identified BMP-2 as an essential factor for the odontoblastic differentiation of DPSCs, by regulating the transcriptional activation of DSPP – a typical dentine-specific protein – through the action of Smads, Dlx5, Runx2, and Msx2 [26,57]. The *in vitro* results of the present study could not confirm any significant additive effect of a single pre-exposure to rhBMP-2 at 100 ng/ml for 24 h – which has been reported [58] to be the optimal concentration and exposure time – on either the expression of osteo/odontogenic markers or the *in vitro* biomineralization potential of DPSCs in both types of scaffolds. The latter is in contrast to previous studies showing the enhanced osteo/odontogenic differentiation and *in vitro* biomineralization potential of dental MSC populations exposed to rhBMP2 [26,57] or transiently transfected to express BMP-2 [59]. Nevertheless, these studies have shown that there is a dose- and time-dependent effect of exogenous BMP-2 application in DPSC cultures, showing a maximum efficacy in triggering odontogenic differentiation via activation of Smad1/5 signaling after 30 min exposure to 300–600 ng/ml BMP-2 [56]. Other studies report on the repeated exposure to the same concentration (100 ng/ml) of BMP-2 every three days to achieve odontogenic differentiation of DPSCs within 7 days [60]. Previous studies have shown the diverse and highly pleiotropic roles of BMPs in regulating the osteo/odontogenic differentiation of different MSC types [61]. It has also been suggested that delivering exogenous rhBMP-2 at a reduced dose in a controlled manner, such as absorption onto apatite-coated chitosan or chondroitin sulfate scaffolds, is more effective in promoting osteogenic differentiation of various MSC populations compared to a burst exposure at higher doses [62]. This might explain the *in vitro* results of this study, together with the fact that the proposed scaffolds were already very effective in inducing osteo/odontogenic differentiation and biomineralization by DPSCs, without any exceptional additive effect from the application of a single rhBMP-2 exposure, other than a significantly higher upregulation of BGLAP and ALP in CS/Gel-0.1 scaffolds and BMP-2 in CS/Gel-1 scaffolds.

In contrast to the *in vitro* data, a remarkable improvement of the *in vivo* mineralization potential could be observed after a single rhBMP-2 pre-exposure of the DPSC/scaffold constructs before subcutaneous transplantation (Figs. 7 and 8), which is in accordance with other *in vivo* studies on the beneficial effects of rhBMP-2 application on dentine [63] and bone regeneration [64]. Among the very limited number of *in vivo* studies on the application of dental MSCs on chitosan-based biopolymers targeting bone regeneration, it is worth mentioning a study by Ge et al. [65] showing efficient bone regeneration by periodontal ligament stem cell-seeded nanohydroxyapatite-chitosan genipin crosslinked scaffolds in a rat calvarial defect model. However, the present study is the first to provide quantitative *in vivo* data on the bone forming potential of variably crosslinked CS/Gel blends. Unlike other bone tissue scaffolds, the proposed scaffolds possess fluorescent properties providing effective ways for imaging the scaffold-cell interface, tracing scaffold degradation and the gradual replacement by cell-produced ECM, as visualized by confocal laser scanning microscopy. The efficiency of rhBMP-2 as a potent osteoinductive factor supported by the *in vivo* results of this study has been also shown by studies in humans for the osseous reconstruction of oral and craniofacial defects or prior to implant placement [66], although postoperative complications attributed to the high rhBMP-2 doses have been also reported [67].

For all the reasons discussed above, the results of the present study obtained by the application of an ectopic, widely applied small animal model of subcutaneous implantation in immunocompromised mice, should be further validated in an orthotopic, alveolar bone defect large animal model, before proceeding into clinical trials in humans. Towards this end, establishment of clinical-grade constructs, by application of serum/xeno-free culturing environments before *in vivo* transplantation, as recently proposed by several authors [7,68] for the safe and efficient expansion of DPSCs, would be of critical importance. In addition, although the second hypothesis of this study has been confirmed by the obtained *in vivo* data, certain limitations arise by the necessity to further validate different rhBMP-2 concentrations, as well as DPSC pre-exposure times, prior *in vivo* application of the constructs. Moreover, other concentrations, as well as types of crosslinking agents of the natural polymer blends used for scaffold fabrication, followed by analysis of the mechanical properties of the regenerated tissues, might also help to further customize the constructs for certain clinical applications, for *e.g.* small *vs.* large alveolar bone defects, as well as ability to preserve the architecture of the overlying soft tissues.

Human DPSCs have been considered ideal for mineralized bone and tooth tissue engineering applications in the craniofacial region due to an array of advantages, such as neural crest

embryological origin, high plasticity, possibility of long-term cultivation and cryopreservation without loss of differentiation ability [7], good interaction with growth factors and scaffolds, as well as ease of harvesting [21] with several studies proving their high potential to regenerate bone-like tissues, both ectopically and around teeth and implants [22]. A number of studies have been conducted using human DPSCs, both alone and in combination with several types of scaffolds, as TE constructs to repair a various bone defects in animal models, and also in human clinical trials [5,20]. However, to our knowledge, no previous studies have applied DPSCs in biomimetic CS/Gel scaffolds to produce tuneable natural matrices targeting the clinical needs of periodontal/peri-implant alveolar bone TE that requires constructs easy to adapt to complex small to medium size defects and able to trigger osseous regeneration within a reasonable time frame not exceeding 6–10 weeks.

5. Conclusions

In this study we focused on the evaluation of the odonto/osteogenic potential of dental pulp stem cells within porous CS/Gel scaffolds using two concentrations of the chemical crosslinking agent glutaraldehyde, 0.1 and 1%v/v, and successfully fabricated two crosslinked scaffolds types, CS/Gel-0.1 and CS/Gel-1, respectively. Both scaffold types were characterized physicochemically and rheologically. *In vitro* assessment reveals that both scaffold types CS/Gel-0.1 and CS/Gel-1 supported cell viability and proliferation, and showed an extensive formation of a hydroxyapatite-rich nanocrystalline calcium phosphate phase. However, differential gene expression levels indicated that the glutaraldehyde concentration significantly affects the expression of specific osteo/odontogenic genes. The CS/Gel-0.1 scaffold type demonstrated a better biological response and was thus included in the *in vivo* investigation in immunocompromised mice, in which DPSCs/scaffold constructs were subcutaneously implanted for 6, 8 and 10 weeks. The results indicate abundant matrix mineralization at all experimental time periods, revealing the time-dependent production of a densely nucleated, nanocrystalline mineralized matrix that was greater in rhBMP-2 pre-induced cells. After 6 weeks of implantation the regenerated mineralized tissues were analysed indicating a significantly higher amount of osteoid, fully mineralized bone, and empty space reduction in the rhBMP-2 pre-induced constructs. These results reveal a promising strategy for orofacial bone reconstruction. Further investigation in orthotopic animal models and clinical proof-of-concept settings in periodontal/peri-implant defects will provide an additional step towards clinical translation.

Authors' contributions

AB designed the study, performed the *in vitro* experiments, participated in the design of the *in vivo* experiments, analyzed and interpreted the data and drafted the manuscript. AG performed the experiments related to the scaffold fabrication and characterization. IG designed, performed and interpreted the *in vivo* experiments and collected the histological data. CB participated in the design and implementation of the *in vivo* experiments and performed the histological staining. OP contributed to the physicochemical characterization, performed and interpreted the XRD and Rietveld analyses experiments. KL performed and interpreted the SEM-EDX and TG experiments. ME analyzed and interpreted data and critically reviewed the manuscript. GCP analyzed and interpreted data and critically reviewed the manuscript. PK analyzed and interpreted data and critically reviewed the manuscript. MC designed the study, supervised and interpreted the experiments, analyzed the data and critically reviewed the manuscript. All authors read and approved the final manuscript.

Acknowledgements

This study was conducted with financial support of the GSRT grant Excellence II (Project: Osteobiomimesis, MIS 525089), the European Union (EU) and National Resources.

REFERENCES

[1] Tang D, Tare RS, Yang LY, Williams DF, Ou KL, Oreffo ROC. Biofabrication of bone tissue: approaches, challenges and translation for bone regeneration. Biomaterials 2016;83:363–82.
[2] Larsson L, Decker AM, Nibali L, Pilipchuk SP, Berglundh T, Giannobile WV. Regenerative medicine for periodontal and peri-implant diseases. J Dent Res 2016;95(3):255–66.
[3] Sculean A, Nikolidakis D, Schwarz F. Regeneration of periodontal tissues: combinations of barrier membranes and grafting materials – biological foundation and preclinical evidence: a systematic review. J Clin Periodontol 2008;35:106–16.
[4] Rao RR, Stegemann JP. Cell-based approaches to the engineering of vascularized bone tissue. Cytotherapy 2013;15(11):1309–22.
[5] Yamada Y, Nakamura S, Ito K, Umemura E, Hara K, Nagasaka T, et al. Injectable bone tissue engineering using expanded mesenchymal stem cells. Stem Cells 2013;31(3):572–80.
[6] Mason S, Tarle SA, Osibin W, Kinfu Y, Kaigler D. Standardization and safety of alveolar bone-derived stem cell isolation. J Dent Res 2014;93(1):55–61.
[7] Bakopoulou A, Apatzidou D, Aggelidou E, Gousopoulou E, Leyhausen G, Volk J, et al. Isolation and prolonged expansion of oral mesenchymal stem cells under clinical-grade, GMP-compliant conditions differentially affects "stemness" properties. Stem Cell Res Ther 2017;8.
[8] Cochran DL, Cobb CM, Bashutski JD, Chun YHP, Lin Z, Mandelaris GA, et al. Emerging regenerative approaches for periodontal reconstruction: a consensus report from the AAP regeneration workshop. J Periodontol 2015;86(2):S153–6.
[9] Chiono V, Pulieri E, Vozzi G, Ciardelli G, Ahluwalia A, Giusti P. Genipin-crosslinked chitosan/gelatin blends for biomedical applications. J Mater Sci Mater Med 2008;19(2):889–98.
[10] Muzzarelli RAA, Mehtedi M, Bottegoni C, Aquili A, Gigante A. Genipin-crosslinked chitosan gels and scaffolds for tissue engineering and regeneration of cartilage and bone. Mar Drugs 2015;13(12):7314–38.
[11] Oryan A, Sahvieh S. Effectiveness of chitosan scaffold in skin, bone and cartilage healing. Int J Biol Macromol 2017;104:1003–11.

[12] Georgopoulou A, Papadogiannis F, Batsali A, Marakis J, Alpantaki K, Eliopoulos AG, et al. Chitosan/gelatin scaffolds support bone regeneration. J Mater Sci Mater Med 2018;29(5).
[13] Santoro M, Tatara AM, Mikos AG. Gelatin carriers for drug and cell delivery in tissue engineering. J Control Release 2014;190:210–8.
[14] Schonwalder SMS, Bally F, Heinke L, Azucena C, Bulut OD, Heissler S, et al. Interaction of human plasma proteins with thin gelatin-based hydrogel films: a QCM-D and ToF-SIMS study. Biomacromolecules 2014;15(7):2398–406.
[15] Oryan A, Alidadi S, Bigham-Sadegh A, Moshiri A. Comparative study on the role of gelatin, chitosan and their combination as tissue engineered scaffolds on healing and regeneration of critical sized bone defects: an in vivo study. J Mater Sci Mater Med 2016;27(10).
[16] Serra IR, Fradique R, Vallejo MCS, Correia TR, Miguel SP, Correia IJ. Production and characterization of chitosan/gelatinip/beta-TCP scaffolds for improved bone tissue regeneration. Mat Sci Eng C Mater 2015;55:592–604.
[17] Chen JN, Chen HA, Li P, Diao HJ, Zhu SY, Dong L, et al. Simultaneous regeneration of articular cartilage and subchondral bone in vivo using MSCs induced by a spatially controlled gene delivery system in bilayered integrated scaffolds. Biomaterials 2011;32(21):4793–805.
[18] Carvalho IC, Mansur HS. Engineered 3D-scaffolds of photocrosslinked chitosan–gelatin hydrogel hybrids for chronic wound dressings and regeneration. Mat Sci Eng C Mater 2017;78:690–705.
[19] Baniasadi H, Ramazani SAA, Mashayekhan S. Fabrication and characterization of conductive chitosan/gelatin-based scaffolds for nerve tissue engineering. Int J Biol Macromol 2015;74:360–6.
[20] Bakopoulou A, About I. Stem cells of dental origin: current research trends and key milestones towards clinical application. Stem Cells Int 2016, http://dx.doi.org/10.1155/2016/4209891.
[21] Egusa H, Sonoyama W, Nishimura M, Atsuta I, Akiyama K. Stem cells in dentistry – part I: stem cell sources. J Prosthodont Res 2012;56(3):151–65.
[22] Ramamoorthi M, Bakkar M, Jordan J, Tran SD. Osteogenic potential of dental mesenchymal stem cells in preclinical studies: a systematic review using modified ARRIVE and CONSORT guidelines. Stem Cells Int 2015, http://dx.doi.org/10.1155/2015/378368.
[23] Kim S, Shin SJ, Song Y, Kim E. In vivo experiments with dental pulp stem cells for pulp–dentin complex regeneration. Mediat Inflamm 2015, http://dx.doi.org/10.1155/2015/409347.
[24] Zhang Y, Zhang MQ. Synthesis and characterization of macroporous chitosan/calcium phosphate composite scaffolds for tissue engineering. J Biomed Mater Res 2001;55(3):304–12.
[25] Bakopoulou A, Papachristou E, Bousnaki M, Hadjichristou C, Kontonasaki E, Theocharidou A, et al. Human treated dentin matrices combined with Zn-doped, Mg-based bioceramic scaffolds and human dental pulp stem cells towards targeted dentin regeneration. Dent Mater 2016;32(8):E159–75.
[26] Yang W, Harris MA, Cui Y, Mishina Y, Harris SE, Gluhak-Heinrich J. Bmp2 is required for odontoblast differentiation and pulp vasculogenesis. J Dent Res 2012;91(1):58–64.
[27] Kilkenny C, Browne WJ, Cuthill IC, Emerson M, Altman DG. Improving bioscience research reporting: the ARRIVE guidelines for reporting animal research. PLoS Biol 2010;8(6).
[28] Charan J, Kantharia ND. How to calculate sample size in animal studies? J Pharmacol Pharmacother 2013;4(4):303–6.
[29] Thein-Han WW, Saikhun J, Pholpramoo C, Misra RD, Kitiyanant Y. Chitosan–gelatin scaffolds for tissue engineering: physico-chemical properties and biological response of buffalo embryonic stem cells and transfectant of GFP-buffalo embryonic stem cells. Acta Biomater 2009;5(9):3453–66.
[30] Chatzinikolaidou M, Rekstyte S, Danilevicius P, Pontikoglou C, Papadaki H, Farsari M, et al. Adhesion and growth of human bone marrow mesenchymal stem cells on precise-geometry 3D organic-inorganic composite scaffolds for bone repair. Mat Sci Eng C Mater 2015;48:301–9.
[31] Hadjicharalambous C, Buyakov A, Buyakova S, Kulkov S, Chatzinikolaidou M. Porous alumina, zirconia and alumina/zirconia for bone repair: fabrication, mechanical and in vitro biological response. Biomed Mater 2015;10(2):025012.
[32] El-Rashidy AA, Roether JA, Harhaus L, Kneser U, Boccaccini AR. Regenerating bone with bioactive glass scaffolds: a review of in vivo studies in bone defect models. Acta Biomater 2017;62:1–28.
[33] Fricain JC, Schlaubitz S, Le Visage C, Arnault I, Derkaoui SM, Siadous R, et al. A nano-hydroxyapatite – pullulan/dextran polysaccharide composite macroporous material for bone tissue engineering. Biomaterials 2013;34(12):2947–59.
[34] Huang Y, Onyeri S, Siewe M, Moshfeghian A, Madihally SV. In vitro characterization of chitosan–gelatin scaffolds for tissue engineering. Biomaterials 2005;26(36):7616–27.
[35] Sahariah P, Masson M. Antimicrobial chitosan and chitosan derivatives: a review of the structure–activity relationship. Biomacromolecules 2017;18(11):3846–68.
[36] Bastian O, Pillay J, Alblas J, Leenen L, Koenderman L, Blokhuis T. Systemic inflammation and fracture healing. J Leukoc Biol 2011;89(5):669–73.
[37] Chatzinikolaidou M, Pontikoglou C, Terzaki K, Kaliva M, Kalyva A, Papadaki E, et al. Recombinant human bone morphogenetic protein 2 (rhBMP-2) immobilized on laser-fabricated 3D scaffolds enhance osteogenesis. Colloids Surf B Biointerfaces 2017;149:233–42.
[38] Zhang Q, Lu HX, Kawazoe N, Chen GP. Preparation of collagen scaffolds with controlled pore structures and improved mechanical property for cartilage tissue engineering. J Bioact Compat Pol 2013;28(5):426–38.
[39] Danilevicius P, Rezende RA, Pereira FD, Selimis A, Kasyanov V, Noritomi PY, et al. Burr-like, laser-made 3D microscaffolds for tissue spheroid encagement. Biointerphases 2015;10(2):021011.
[40] Liu IH, Chang SH, Lin HY. Chitosan-based hydrogel tissue scaffolds made by 3D plotting promotes osteoblast proliferation and mineralization. Biomed Mater 2015;10(3).
[41] Skarmoutsou A, Lolas G, Charitidis CA, Chatzinikolaidou M, Vamvakaki M, Farsari M. Nanomechanical properties of hybrid coatings for bone tissue engineering. J Mech Behav Biomed Mater 2013;25:48–62.
[42] Cheng NC, Wang S, Young TH. The influence of spheroid formation of human adipose-derived stem cells on chitosan films on sternness and differentiation capabilities. Biomaterials 2012;33(6):1748–58.
[43] Yeh HY, Liu BH, Sieber M, Hsu SH. Substrate-dependent gene regulation of self-assembled human MSC spheroids on chitosan membranes. BMC Genomics 2014;15.
[44] Hsu SH, Huang GS, Feng F. Isolation of the multipotent MSC subpopulation from human gingival fibroblasts by culturing on chitosan membranes. Biomaterials 2012;33(9):2642–55.
[45] Asghari Sana F, Capkin Yurtsever M, Kaynak Bayrak G, Tuncay EO, Kiremitci AS, Gumusderelioglu M. Spreading, proliferation and differentiation of human dental pulp stem cells on chitosan scaffolds immobilized with RGD or fibronectin. Cytotechnology 2017;69(4):617–30.
[46] Tsai WB, Chen YR, Liu HL, Lai JY. Fabrication of UV-crosslinked chitosan scaffolds with conjugation of RGD

peptides for bone tissue engineering. Carbohyd Polym 2011;85(1):129–37.
[47] Oryan A, Kamali A, Moshiri A, Baharvand H, Daemi H. Chemical crosslinking of biopolymeric scaffolds: current knowledge and future directions of crosslinked engineered bone scaffolds. Int J Biol Macromol 2018;107:678–88.
[48] Chajra H, Rousseau CF, Cortial D, Ronziere MC, Herbage D, Mallein-Gerin F, et al. Collagen-based biomaterials and cartilage engineering. Application to osteochondral defects. Bio Med Mater Eng 2008;18:S33–45.
[49] Guldner NW, Jasmund I, Zimmermann H, Heinlein M, Girndt B, Meier V, et al. Detoxification and endothelialization of glutaraldehyde-fixed bovine pericardium with titanium coating a new technology for cardiovascular tissue engineering. Circulation 2009;119(12):1653–60.
[50] Costa ED, Pereira MM, Mansur HS. Properties and biocompatibility of chitosan films modified by blending with PVA and chemically crosslinked. J Mater Sci Mater Med 2009;20(2):553–61.
[51] Sculean A, Nikolidakis D, Nikou G, Ivanovic A, Chapple ILC, Stavropoulos A. Biomaterials for promoting periodontal regeneration in human intrabony defects: a systematic review. Periodontology 2000 2015;68(1):182–216.
[52] Bachtiar EW, Amir LR, Suhardi P, Abas B. Scaffold degradation during bone tissue reconstruction in *Macaca nemestrina* mandible. Interv Med Appl Sci 2016;8(2):77–81.
[53] Chen Y, Zhang F, Fu Q, Liu Y, Wang Z, Qi N. In vitro proliferation and osteogenic differentiation of human dental pulp stem cells in injectable thermo-sensitive chitosan/beta-glycerophosphate/hydroxyapatite hydrogel. J Biomater Appl 2016;31(3):317–27.
[54] Frohbergh ME, Katsman A, Mondrinos MJ, Stabler CT, Hankenson KD, Oristaglio JT, et al. Osseointegrative properties of electrospun hydroxyapatite-containing nanofibrous chitosan scaffolds. Tissue Eng Pt A 2015;21(5–6):970–81.
[55] Gerhardt LC, Boccaccini AR. Bioactive glass and glass-ceramic scaffolds for bone tissue engineering. Materials 2010;3(7):3867–910.
[56] Anusuya GS, Kandasamy M, Jacob Raja SA, Sabarinathan S, Ravishankar P, Kandhasamy B. Bone morphogenetic proteins: signaling periodontal bone regeneration and repair. J Pharm Bioallied Sci 2016;8(Suppl. 1):S39–41.
[57] Qin W, Yang F, Deng R, Li DD, Song Z, Tian YG, et al. Smad 1/5 is involved in bone morphogenetic protein-2-induced odontoblastic differentiation in human dental pulp cells. J Endodont 2012;38(1):66–71.
[58] Casagrande L, Demarco FF, Zhang Z, Araujo FB, Shi S, Nor JE. Dentin-derived BMP-2 and odontoblast differentiation. J Dent Res 2010;89(6):603–8.
[59] Yang X, van der Kraan PM, Bian Z, Fan M, Walboomers XF, Jansen JA. Mineralized tissue formation by BMP2-transfected pulp stem cells. J Dent Res 2009;88(11):1020–5.
[60] Qin W, Liu PC, Zhang R, Huang SH, Gao XL, Song Z, et al. JNK MAPK is involved in BMP-2-induced odontoblastic differentiation of human dental pulp cells. Connect Tissue Res 2014;55(3):217–24.
[61] Zhang F, Song J, Zhang H, Huang E, Song D, Tollemar V, et al. Wnt and BMP signaling crosstalk in regulating dental stem cells: implications in dental tissue engineering. Genes Dis 2016;3(4):263–76.
[62] Shim JH, Kim SE, Park JY, Kundu J, Kim SW, Kang SS, et al. Three-dimensional printing of rhBMP-2-loaded scaffolds with long-term delivery for enhanced bone regeneration in a rabbit diaphyseal defect. Tissue Eng Pt A 2014;20(13–14):1980–92.
[63] Iohara K, Nakashima M, Ito M, Ishikawa M, Nakasima A, Akamine A. Dentin regeneration by dental pulp stem cell therapy with recombinant human bone morphogenetic protein 2. J Dent Res 2004;83(8):590–5.
[64] Liu HC, E L-L, Wang D-S, Su F, Wu X, Shi Z-P, Lv Y, Wang J-Z. Reconstruction of alveolar bone defects using bone morphogenetic protein 2 mediated rabbit dental pulp stem cells seeded on nano-hydroxyapatite/collagen/poly(L-lactide). Tissue Eng Pt A 2011;17(19–20):2417–33.
[65] Ge SH, Zhao N, Wang L, Yu MJ, Liu H, Song AM, et al. Bone repair by periodontal ligament stem cell-seeded nanohydroxyapatite-chitosan scaffold. Int J Nanomed 2012;7:5405–14.
[66] de Queiroz Fernandes J, de Lima VN, Bonardi JP, Filho OM, Queiroz SBF. Bone regeneration with recombinant human bone morphogenetic protein 2: a systematic review. J Maxillofac Oral Surg 2018;17(1):13–8.
[67] Reuss JM, Pi-Anfruns J, Moy PK. Is bone morphogenetic protein-2 as effective as alveolar distraction osteogenesis for vertical bone regeneration? J Oral Maxil Surg 2018;76(4):752–60.
[68] Xiao JY, Yang DW, Li QW, Tian WD, Guo WH. The establishment of a chemically defined serum-free culture system for human dental pulp stem cells. Stem Cell Res Ther 2018;9.